CHAPTER 3

THE DISCRETE REACTION FIELD APPROACH FOR CALCULATING SOLVENT EFFECTS

PIET TH. VAN DUIJNEN[1], MARCEL SWART[2], AND LASSE JENSEN[3]

[1]*Zernike Institute for Advanced Materials, Rijksuniversiteit Groningen, Nijenborgh 4, 9747 AG, Groningen, The Netherlands, e-mail: p.t.van.duijnen@rug.nl*

[2]*Institució Catalana de Recerca i Estudis Avançats (ICREA), 08010 Barcelona, Spain and Institut de Química Computacional, Universitat de Girona, Campus Montilivi, 17071 Girona, Spain, e-mail: marcel.swart@udg.edu*

[3]*Department of Chemistry, The Pennsylvania State University, University Park, PA 16802, USA, e-mail: jensen@chem.psu.edu*

Abstract: We present here the discrete reaction field (DRF) approach, which is an accurate and efficient model for studying solvent effects on spectra, chemical reactions, solute properties, etc. The DRF approach uses a polarizable force field, which is (apart from the short-range repulsion) based entirely on second-order perturbation theory, and therefore ensures the correct analytical form of model potentials. The individual interaction components are modeled independently from each other, in a rigorous and straightforward way. The required force field parameters result as much as possible from quantum-chemical calculations and on monomer properties, thereby avoiding undesired fitting of these parameters to empirical data.

Because the physical description is correct and consistent, the method allows for arbitrary division of a system into different subsystems, which may be described either on the quantum-mechanical (QM) or the molecular mechanics (MM) level, without significant loss of accuracy. This allows for performing fully MM molecular simulations (Monte Carlo, molecular dynamics), which can subsequently be followed by performing QM/MM calculations on a selected number of representative snapshots from these simulations. These QM/MM calculations then give directly the solvent effects on emission or absorption spectra, molecular properties, organic reactions, etc

3.1. INTRODUCTION

Ballhausen said once, starting his lecture on the Jahn–Teller effect: 'The Jahn–Teller effect does not exist' [1]. J–T, relativistic and quantum effects exist by the grace of incomplete descriptions of systems under study. In contrast, solvent effects are real and part of everyday life of the majority of chemists.

Hence accounting for solvent effects in computational chemistry—or in general, the modeling of molecular properties in the condensed phase—is of paramount

S. Canuto (ed.), Solvation Effects on Molecules and Biomolecules, 39–102.
DOI 10.1007/978-1-4020-8270-2_3,

importance because chemistry overwhelmingly takes place in solution, and molecular properties differ in that environment often considerably in comparison with the gas phase. From a computational chemical point of view, the focus will be on a single molecule (or a molecular system) while the solvent effects are treated as perturbations of the molecular system. The latter (the solute) is then treated with some quantum-mechanical (QM) method while the rest is treated by a much simpler, usually classical, method [2,3,4,5,6,7,8,9,10,11,12,13,14,15,16,17,18].

The classical descriptions can in general be divided into two groups depending on the detail in which the solvent is considered. The first group consists of the continuum models [7,9,14,15] in which the solvent is treated as a continuous medium characterized only by its dielectric constant. Because of their efficiency in terms of computer demands, these methods still dominate the field of computing solvent effects. However, the microscopic structure of the solvent and specific interactions are here completely neglected and therefore provide a poor description of short-range interactions. Moreover, the size and the shape of the cavity in which the solute is embedded affect the results [19]. An ab initio approach for choosing the solvent radius (taking it from the macroscopic density and molecular mass of the solvent) [20] has been suggested recently to avoid ambiguities with empirically adapted solvent radii. However, since the boundary is in principle arbitrary the charge distribution of the solute in all practical cases will extend into the continuum. In particular Chipman [21] but also Mennucci [22] and Cossi [23] discuss this charge penetration and describe methods to account for it. These improvements will make the straight continuum approaches less dependent on the actual size and shape of the cavity. Nevertheless some formal problems will remain. (See Figure 3-1) First, a dielectric continuum can only stabilize a charge distribution and the more so the closer the charges are to the cavity boundary (or it does nothing: for an infinite large cavity, or for $\varepsilon = 1$). This means that the interactions of the electrons of a solute will be larger than that of the nuclei because the former are on average closer to that boundary. The electronic charge distribution will therefore be inflated with respect to the gas phase situation, an effect that is not without consequences [24]. Next, in general the continuum is

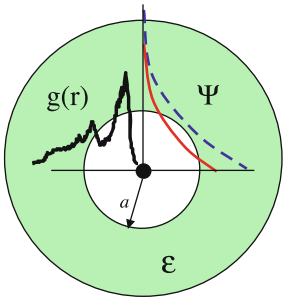

Figure 3-1. Schematic representation of atom in dielectric continuum. Ψ: wave function in vacuo (*solid line*) and solvated (*dashed line*); ε: dielectric constant ; a: cavity radius; $g(r)$: radial distribution of solvent molecules

assumed homogeneous, which should force the cavity to go beyond the second maximum of $g(r)$. Finally, the dielectric constant is a macroscopic property connected with the polarization of the solvent, i.e., with the time- and space-averaged (induced) dipoles. The solute–solvent interaction then will be of type $<\rho_{\text{solute}}> \Leftrightarrow <M_{\text{solvent}}>$, i.e., the average charge density (ρ) interacts with the averaged dipoles (M) of the environment, while in actual experiments results are obtained as (averaged) instantaneous interactions, i.e., of type $<\rho_{\text{solute}} \Leftrightarrow M_{\text{solvent}}>$ which are in general different from the former.

An extension of the continuum model is the inclusion of explicit solvent molecules in the cavity—treated fully quantum-mechanically together with the solute—in order to get a better grip on specific interactions like hydrogen bonding. The best approach to this is to take two or three solvation shells. Of course, some statistical mechanics procedure is needed in order to obtain a reasonable solvent distribution $g(r)$, and that puts this approach into the field of mixed quantum-classical mechanical (QM/MM) models. An early application of this model [25] revealed that only the interaction between the solute and the continuum survives statistically. By adding sufficient solvent shells and increasing the cavity size accordingly, this interaction can be made arbitrarily small, thus making the presence of the continuum superfluous [24,26].

To the second group belong the discrete solvent models in which one or more solvent molecules are treated explicitly. Among these are the supermolecular model [27], the frozen density functional approach [28], ab initio molecular dynamics (AIMD) [29] and the combined quantum and molecular mechanics (QM/MM) models [2,3,4,5,6,8,10,13,18,30,31,32]. In both the supermolecular and the AIMD models all molecules are treated on the same level of theory. This can give highly accurate descriptions of the solute–solvent interactions but due to the computational demands it becomes rapidly impractical so that either only a few of the (small) solvent molecules can be included or the actual level—QM method, basis sets—has to be reduced. Moreover, the definition of the molecular properties requires an arbitrary partitioning of the wave function or the density among the molecules, much in the same way as is necessary for defining atomic charges. Due to this arbitrariness molecular properties cannot be defined for individual molecules [33,34,35] and will depend on the particular partitioning employed. This is for instance shown in an AIMD study of ice I_h [33], where it was found that the average dipole moment ranges from 2.3 to 3.1 D.

In the QM/MM method the system is usually a priori divided into QM (the solute) and classical (MM, the solvent) parts, and an effective operator describes the interaction between the two subsystems. The solvent molecules are treated with a 'classical' force field ('classical' meaning that there are no elementary particles or quantum 'effects') that opens the possibility to take a much larger number of solvent molecules into account. Optionally, the whole system can be embedded in a continuum, e.g., for taking large-range interactions into account. Similar to the continuum approach, the solute is separated from the solvent and its molecular properties are therefore well defined. The remaining problem is to find an accurate approximate representation of

the solvent molecules, the solute–solvent and the solvent–solvent interactions [36]. The discrete representation of the solvent molecules requires sampling of the degrees of freedom of the solvent. This is typically done using Monte Carlo (MC) or molecular dynamics (MD) techniques to generate a large number of possible solvent configurations. This leads to many QM/MM calculations for the solute's properties which must be averaged or represented in another way. Hence the QM/MM method is often employed at a semi-empirical level of the QM theory.

The force fields used in the QM/MM methods are typically adopted from fully classical force fields. While this is in general suitable for the solvent–solvent interactions it is not clear how to model, e.g., the van der Waals interaction between the solute and the solvent. The van der Waals interactions are typically treated as Lennard-Jones (LJ) potentials with parameters for the quantum atoms taken from the classical force field or optimized for the particular QM/MM method for some molecular complexes. However, it is not certain that optimizing the (dispersion and short-range repulsion) parameters on small complexes will improve the results in a QM/MM simulation of liquids [37].

Classical force fields that take polarization into account explicitly, the so-called polarizable force fields [2,3,11,31,32,38,39,40,41,42,43,44,45,46,47,48,49,50,51, 52,53], were originally not popular. The arguments against using them are mostly based on 'efficiency' in terms of computing times. Energy contributions of about 10% to the interaction of (up to) trimers [40,41] were considered of no consequence: instead, polarization in simulations of, e.g., liquid water was taken care of by increasing the monomer dipole moment from the experimental gas phase value of 1.86 D to its condensed phase value of about 2.7 D [40]. Refining this in order to get better agreement with details of the radial distribution led, e.g., to the TIP4P model [54]. Recently the trend is to use (ab initio) QM calculations as a guide, instead of fitting force field parameters (of total energy expressions) to experimental results.

Nowadays, the interest in polarizable force fields has regained ground, both for purely classical and QM/MM simulations. It was shown that it is important to consider also the polarization of the solvent molecules [40,55,56]. Since the inclusion of the solvent polarization leads naturally to an increase in computational time, most studies still ignore this contribution and use the more simple 'effective' pair potentials. If the solvent polarization is included it is usually treated using either an isotropic molecular polarizability [11,39,52] or using distributed atomic polarizabilities [31,32,46,49,53] according to the Applequist scheme [57,58,59]. However, at short distances the Applequist scheme leads to the so-called 'polarization catastrophe' due to the use of a classical description in the bonding regions. Thole [59] avoided this problem by introducing smeared out dipoles, which mimic the overlapping of charge distributions at short distances. Thole's model, which will be discussed in detail later, has been shown to be quite successful in reproducing molecular polarizability tensors using model atomic polarizability parameters independent of the chemical environment of the atoms [59,60]. Karlström et al. [18,36] have a different approach in which solute–solvent and solvent–solvent interactions—including

polarization, dispersion and short-range repulsion—are modeled based on specific QM calculations by keeping a large amount of 'orbital' information.

Recently, we have seen a renewed interest in the development and application of polarizable force fields [61,62,63,64,65,66]. Although these studies are all concerned with a proper description of polarization effects in chemical systems, the philosophy behind the approaches is sometimes substantially different from Thole's. In the paper by Mooij et al. [61], the separate energy terms have a well-defined physical meaning, which enhances transferability to other molecules. Moreover, the parameters were obtained from ab initio calculations on the level of Møller–Plesset second-order perturbation theory (MP2) [67] using large basis sets and corrected for the basis set superposition error (BSSE). In contrast Kaminski et al. [62] fitted atomic polarizabilities either to the change in electrostatic potential (ESP) at a set of grid points outside the van der Waals surface of the molecule or to three-body energies of five small molecules [64]. The use of fitting on a grid, in their first study, makes the polarizabilities depend on the choice of the grid, a similar problem met with ESP charges [48,68,69,70]. In their second paper [64] it is unclear which method has been used to obtain the 'three-body' energies and whether the results have been corrected for BSSE. More importantly, their 'three-body' energies are obtained from intramolecular polarization only, while three-body energies usually concern intermolecular interactions [71], and the polarizabilities will be used to describe intermolecular interactions. One of the main objections to studies such as those by Kaminski et al. [62,64] is that the polarizability enters as a fitting parameter, thereby ignoring the fact that the polarizability is an intrinsic property of an atom or molecule. This is in contrast to the two other papers [61,63], as well as previous work in our group [59].

Without any doubt the most advanced force field is the water potential of Bukowski et al. [72] containing pairwise and many-body interactions and describing the interactions with an accuracy < 0.07 kcal/mol and predicting the properties of the water dimer and of liquid water in excellent agreement with experiments. But it requires 2510 grid points and clusters of up to 32 monomers, CCSD(T) calculations in quadruple-zeta basis (QZ++) to fit all the parameters, and it is highly specific. This is obviously beyond practical use for the large (bio-)organic molecules we have in mind, and for that purpose it is more advantageous to use the transferable model potentials like the polarizable force field used in our group.

In general, the interaction between two systems, having a geometry symbolically represented by **R,** is written as

$$\begin{aligned}\Delta U_{QS}^{\text{int}}(\mathbf{R}) = U_{QS}(\mathbf{R}) - (U_Q^0 + U_S^0) = \Delta U_{QS}^{\text{elst}}(\mathbf{R}) + \Delta U_{QS}^{\text{pol}}(\mathbf{R}) \\ + \Delta U_{QS}^{\text{disp}}(\mathbf{R}) + \Delta U_{QS}^{\text{rep}}(\mathbf{R})\end{aligned} \tag{3-1}$$

with U_{QS} the total energy of the QS system, U_X^0 the ground state energy of system X, $\Delta U_{QS}^{\text{elst}}$, $\Delta U_{QS}^{\text{pol}}$, $\Delta U_{QS}^{\text{disp}}$ and $\Delta U_{QS}^{\text{rep}}$, respectively the electrostatic, polarization, dispersion and (short-range) repulsion energies between two subsystems Q and S.

For multi-molecular assemblies one has to consider whether the total interaction energy can be written as the sum of pairwise interactions. The first-order electrostatic interaction is exactly pairwise additive, the dispersion only up to second order (in third order a generally small three-body Axilrod–Teller term appears [73]) while the induction is not at all pairwise: it is non-linearly additive due to the interference of electric fields from different sources. Moreover, for polar systems the inducing fields are strong enough to change the molecular wave functions significantly.

Fitting of model potentials to supermolecular interactions like in Eq. (3-1) has its disadvantages: the calculations have to be repeated many times and a predefined analytical expression of the model potentials in terms of atomic parameters is required. These parameters are not easily transferred to other situations. The internal state of, e.g., system A depends on the presence of another system *X*, and this will be different near system *Y*. Furthermore, the chosen analytical form of the potential may give rise to problems and errors. For example, Hartree–Fock (HF) calculations fitted to a power series in $1/r$ suggest that the $1/r^6$ terms have to do with dispersion, which is not part of the HF energy. Finally, such empirical potentials are best for describing situations close to those to which the parameters are fitted. Whenever the situation is very different from that, the results will be doubtful.

Our QM/MM model—the discrete (or direct) reaction field (DRF) model—treats the various terms in Eq. (3-1) separately and on the basis of their own intrinsic physical meaning [3,10,31,32,38,59,74]. Historically, DRF was developed to study biochemical problems, in particular for unraveling the reaction mechanism of papain. For that we went stepwise from a model active site [75] to a model active site plus a point charge representation of an α-helix [76,77,78], then to a model with a polarizable helix [78,79], and finally to an all-atom treatment of the enzyme [41]. Furthermore, we extended these studies with an exercise—with the continuum version—to show that a solvent-exposed residue has no effect on the reaction mechanism [80]. Up to then we considered the protein as a peculiar solvent; the 'real' solvents, requiring extensive MC or MD simulations, came later.

In most cases we apply now the method—coined by Coutinho and Canuto [81,82] as *sequential* MC (SMC) or *sequential* MD (SMD)—in which an all-classical simulation is performed from which, after equilibration, a relative small number of snapshots of uncorrelated solute–solvent configurations are collected. In Ref. [81] these authors show that a relatively small number of configurations—small with respect to the total number generated in the simulation—contains all statistically relevant information. Then from QM or QM/MM calculations on the snapshots the (electronic) molecular properties in solution are obtained by averaging, or otherwise collected. In the original paper the saved solute–solvent configurations were subjected to an all-QM calculation. We apply this technique generally with only the solute as QM part for reasons already mentioned above.

The total Hamiltonian in QM/MM is as usual written as

$$\hat{H}(\mathbf{r}_q) = \hat{H}^0(\mathbf{r}_q) + \hat{H}_{QM/MM}(\mathbf{r}_q, \mathbf{r}_s) + \hat{H}_{MM}(\mathbf{r}_s) \tag{3-2}$$

with $\hat{H}^0(\mathbf{r}_q)$ the vacuum Hamiltonian of the QM part, $\hat{H}_{MM}(\mathbf{r}_s)$ the Hamiltonian of the MM part and $\hat{H}_{QM/MM}(\mathbf{r}_q, \mathbf{r}_s)$ the operator describing the interaction between the QM and MM particles. We note that the last two operators contain electrostatic, many-body polarization, short-range repulsion and dispersion terms. Electrostatic potentials are modeled with point charges on atoms (or, if necessary, on additional points, obtained from QM calculations), while polarization and dispersion are described in terms of (model) atomic polarizabilities resulting from calculations or experiment. We want the parameters in the model Hamiltonians to be transferable, and requiring no fitting to energies, structures or thermodynamical properties of the system under study. The parameters of DRF are therefore based on properties of monomers or, if monomers are too large, of model subsystems, and on second-order perturbation theory. The only term so far not coming from perturbation theory is the short-range repulsion, which we have borrowed from other force fields.

The QM/MM version of DRF has been implemented in HONDO [83], ZINDO [84], GAMESS [85] and ADF [86] while DRF90 [87] is our classical statistical mechanics package.

In Section 2 we give the theoretical background and implementation of DRF and in Section 3 some examples to validate the model. Section 4 is dedicated to applications where we address a wide variety of solvent effects.

3.2. THEORY

3.2.1. Perturbation Theory

In a quantum-chemical description of the two subsystems Q and S of the preceding section the total wave function—in the long-range approximation—can be written as

$$\Psi_{QS}(\mathbf{r}_q, \mathbf{r}_s) = \Psi_Q(\mathbf{r}_q) \otimes \Psi_S(\mathbf{r}_s) \tag{3-3}$$

where Ψ_X is the wave function and $\mathbf{r}_X$ the coordinates of particles of system X. Since the short-range repulsion ($\Delta U^{\text{rep}}_{QS}$, cf. Eq. 3-1) in this approximation vanishes, and the total energy of the system is obtained as

$$U_{Q+S} = \left\langle \Psi_Q \Psi_S \right| \hat{H}^0_Q + \hat{H}^0_S + \hat{V}_{QS} \left| \Psi_Q \Psi_S \right\rangle \tag{3-4}$$

where $\hat{H}^0_Q(\mathbf{r}_q)$ and $\hat{H}^0_S(\mathbf{r}_s)$ are the Hamiltonians of the isolated systems and

$$\hat{V}_{QS} = \sum_{\substack{q \in Q \\ s \in S}} \frac{z_q z_s}{|\mathbf{r}_q - \mathbf{r}_s|}. \tag{3-5}$$

the interaction operator, with $\{z\}$ the charges (electrons, nuclei) in the system. Because the overlap is negligible, the integrations involved in Eq. (3-4) can be evaluated locally, e.g.,

$$\Delta U_{\text{int}} = \left\langle \Psi_Q(\mathbf{r}_q) \left| \sum_{q\in Q} z_q \, \langle \Psi_S(\mathbf{r}_s)| \sum_{s\in S} \frac{z_s}{|\mathbf{r}_q - \mathbf{r}_s|} \, |\Psi_S(\mathbf{r}_s)\rangle_S \right| \Psi_Q(\mathbf{r}_q) \right\rangle_Q$$
$$= \left\langle \Psi_Q(\mathbf{r}_q) \left| \sum_{q\in Q} z_q \hat{V}_S(\mathbf{r}_q) \right| \Psi_Q(\mathbf{r}_q) \right\rangle_Q \tag{3-6}$$

so that the problem of Eq. (3-4) is partitioned into smaller ones, for which the equations can be written as

$$U_{QS} = \left\langle \Psi_Q(\mathbf{r}_q) \left| \hat{H}^0_Q(\mathbf{r}_q) + \hat{V}^0_S(\mathbf{r}_q) \right| \Psi_Q(\mathbf{r}_q) \right\rangle = U^0_Q + \Delta U_{\text{int}} \tag{3-7}$$

which is equivalent to solving a Schrödinger equation for system Q in an external potential. The result, Ψ_Q, can obviously be used to define an *effective* potential on S,

$$\hat{V}_Q(r_s) = \left\langle \Psi_Q(\mathbf{r}_q) \right| \sum_{s\in S} \frac{z_q}{|\mathbf{r}_q - \mathbf{r}_s|} \left| \Psi_Q(\mathbf{r}_q) \right\rangle_Q \tag{3-8}$$

leading to a new $\Psi'_S(\mathbf{r}_s)$, etc., a process that can be repeated until self-consistency. This is a simplified sketch of the group function approach originally described by McWeeny [88] and reformulated for non-orthogonal groups by Mehler [89,90,91].

It is better to analyze the interaction energy by means of perturbation theory (PT) [92,93,94,95,96] not only because ΔU_{int} is in general much smaller than the intramolecular U^0_X, but mainly because PT sets the correct analytical form of possible model potentials. Up to second order we have

$$\Delta U^{(1)}_{\text{int}} = \left\langle \Psi^0_Q \Psi^0_S \left| V_{QS} \right| \Psi^0_Q \Psi^0_S \right\rangle \tag{3-9}$$

$$\Delta U^{(2)}_{\text{ind}} = \sum_{k\neq 0} \frac{\left| \left\langle \Psi^0_Q \Psi^0_S \right| V_{QS} \left| \Psi^k_Q \Psi^0_S \right\rangle \right|^2}{U^0_Q - U^k_Q} + \sum_{l\neq 0} \frac{\left| \left\langle \Psi^0_Q \Psi^0_S \right| V_{QS} \left| \Psi^0_Q \Psi^l_S \right\rangle \right|^2}{U^0_S - U^l_S} \tag{3-10}$$

$$\Delta U^{(2)}_{\text{disp}} = \sum_{k,l\neq 0} \frac{\left| \left\langle \Psi^0_Q \Psi^0_S \right| V_{QS} \left| \Psi^k_Q \Psi^l_S \right\rangle \right|^2}{U^0_Q - U^k_Q + U^0_S - U^l_S} \tag{3-11}$$

where U^n_X is the nth excited state of system X. Introducing the multipole expansion about a center $\mathbf{x}$ of the Coulomb potential of X at $\mathbf{y}$:

$$\frac{1}{|\mathbf{r}_y - \mathbf{r}_x|} = \sum_n \left(\frac{1}{n!} \right) T^{(n)}_{yx,\eta_1,\eta_2,\ldots,\eta_n} \tag{3-12}$$

with $T^{(n)}_{xy,\eta_1,\eta_{2,\ldots},\eta_n} = \nabla_{xy,\eta_1} \ldots \nabla_{yx,\eta_n} \left(1/R_{xy}\right)$

$$\begin{aligned} T^{(0)}_{yX} &= \frac{1}{|\mathbf{r}_y - \mathbf{x}|} \;;\; T^{(1)}_{\mathrm{yX},\eta} = -\frac{\left(r_y - x\right)_\eta}{|\mathbf{r}_y - \mathbf{x}|^3} \;; \\ T^{(2)}_{yX,\eta\vartheta} &= \frac{3\left(r_y - x\right)_\eta \left(r_y - x\right)_\vartheta}{|\mathbf{r}_y - \mathbf{x}|^5} - \frac{\delta_{\eta\vartheta}}{|\mathbf{r}_y - \mathbf{x}|^3} \end{aligned} \tag{3-13}$$

Inserting the expansion in the second term in Eq. (3-10) leads to

$$\begin{aligned} &\sum_{l\neq 0} \frac{\left|\left\langle \Psi^0_Q \Psi^0_S | V_{QS} | \Psi^0_Q \Psi^l_S \right\rangle\right|^2}{U^0_S - U^l_S} = \sum_{l\neq 0} \frac{\left|\left\langle \Psi^0_Q \Psi^0_S | \mathbf{T}^{(1)}_{sQ}(\mathbf{r}_q - \mathbf{q}) | \Psi^0_Q \Psi^l_S \right\rangle\right|^2}{U^0_S - U^l_S} \\ &= \left|\left\langle \Psi^0_Q \left| \left(\frac{(\mathbf{r}_q - \mathbf{s})}{|\mathbf{r}_q - \mathbf{s}|^3}\right) \right| \Psi^0_Q \right\rangle\right|^2 \sum_{l\neq 0} \frac{\left|\left\langle \Psi^0_S | (\mathbf{r}_q - \mathbf{q}) | \Psi^l \right\rangle\right|^2}{U^0_S - U^l_S} \\ &= -\frac{1}{2} \left\langle \mathbf{e}_Q(\mathbf{s}) \right\rangle^2 \boldsymbol{\alpha}_S \end{aligned} \tag{3-14}$$

and, hence,

$$\Delta U^{(2)}_{ind} = -\frac{1}{2} \left\langle \mathbf{e}_S(\mathbf{q}) \right\rangle^2 \boldsymbol{\alpha}_Q(\mathbf{q}) - \frac{1}{2} \left\langle \mathbf{e}_Q(\mathbf{s}) \right\rangle^2 \boldsymbol{\alpha}_s(\mathbf{s}) \tag{3-15}$$

where $\mathbf{e}_X(\mathbf{y})$ is the electric field at $\mathbf{y}$ due to the charge distribution of system X, and $\alpha_X(\mathbf{x})$ the polarizability of X centered at $\mathbf{x}$.

The dispersion interaction arises from fluctuations in the charge distribution of Q, leading to transient induction in S and vice versa. By applying the multipole expansion in the dipole approximation in both Q and S, $\Delta U^{(2)}_{disp}$ is reduced to

$$\begin{aligned} \Delta U^{(2)}_{disp} &= \sum_{k,l\neq 0} \frac{\left|\left\langle \Psi^0_Q \Psi^0_S | \mathbf{T}^{(2)}_{sS} \mathbf{T}^{(2)}_{qQ}(\mathbf{r}_s - \mathbf{s})(\mathbf{r}_q - \mathbf{q}) | \Psi^k_Q \Psi^l_S \right\rangle\right|^2}{U^0_Q - U^k_Q + U^0_S - U^l_S} \\ &= \frac{1}{|\mathbf{s} - \mathbf{q}|^6} \left\{ \frac{3\left(\mathbf{s} - \mathbf{q}\right)\left(\mathbf{s} - \mathbf{q}\right)}{|\mathbf{s} - \mathbf{q}|^2} + \mathbf{I} \right\} \\ &\quad \times \sum_{k,l\neq 0} \frac{\left|\left\langle \Psi^0_Q | (\mathbf{r}_q - \mathbf{q}) | \Psi^k_Q \right\rangle\right|^2 \left|\left\langle \Psi^0_S | (\mathbf{r}_s - \mathbf{s}) | \Psi^l_S \right\rangle\right|^2}{U^0_Q - U^k_Q + U^0_S - U^l_S} \end{aligned} \tag{3-16}$$

Due to the excitation energies of both S and Q in the denominator the local integrations do not lead directly to monomer factors, but by invoking the Unsöld approximation [97] it is possible to split the denominator into a product:

$$\frac{1}{U_Q^0 - U_Q^k + U_S^0 - U_S^l} = \left(\frac{\Delta_S \Delta_Q}{\Delta_S + \Delta_Q}\right) \times \left[\frac{-1}{\left(U_Q^0 - U_Q^k\right)\left(U_S^0 - U_S^l\right)}\right] \{1 + \Delta_{kl}\} \tag{3-17}$$

where Δ_S and Δ_Q are chosen so as to minimize the error Δ_{kl}. The expression for the dispersion can hence again be expressed in terms of the polarizabilities of Q and S, leading to the well-known London approximation [98]:

$$\Delta U_{disp}^{(2)} \approx \frac{1}{|\mathbf{s} - \mathbf{q}|^6} \times \left(\frac{\Delta_S \Delta_Q}{\Delta_S + \Delta_Q}\right) \times \frac{1}{2}\boldsymbol{\alpha}_Q \left\{\frac{3\,(\mathbf{s} - \mathbf{q})\,(\mathbf{s} - \mathbf{q})}{|\mathbf{s} - \mathbf{q}|^2} + \mathbf{I}\right\} \frac{1}{2}\boldsymbol{\alpha}_S \tag{3-18}$$

where $\mathbf{I}$ is the 3×3 unit matrix. Another way to write the dispersion energy is the Casimir–Polder integral [99]

$$\Delta U_{disp}^{(2)} = T_{sq,\eta\tau} T_{sq,\xi\theta} \lim_{x \to \infty} \int \alpha_{Q,\eta\xi}(\mathrm{i}u)\alpha_{S,\tau\theta}(\mathrm{i}u)\mathrm{du} + \text{higher order terms} \tag{3-19}$$

where $\alpha(\mathrm{i}u)$ is the frequency-dependent dipole polarizability at imaginary frequency $\omega = \mathrm{i}u$. By inserting $\alpha(\omega) \approx \frac{n_v(0)}{n_v - \omega^2}$, where n_v the number of valence electrons, in Eq. (3-19) and averaging rotationally, the Slater–Kirkwood approximation [96] is obtained:

$$\Delta U_{disp}^{Slater-Kirkwood} = -\frac{3}{2}\frac{1}{|\mathbf{s} - \mathbf{q}|^6}\frac{\alpha_S \alpha_Q}{\sqrt{(\alpha_S / n_{S,v})} + \sqrt{(\alpha_Q / n_{Q,v})}} \tag{3-20}$$

A semi-classical estimate is obtained by dropping the excitation energy of one of the systems in the denominator in Eq. (3-11), assuming instantaneous instead of frequency-dependent interaction. Then, by means of the closure relation, it is easy to show that in the dipole approximation Eq. (3-11) transforms into [3,38]

$$\Delta U_{disp}^{sc} = -\frac{1}{2}\left\{\mathbf{e_Q}\boldsymbol{\alpha}_S\mathbf{e}_Q \rangle - \langle \mathbf{e}_Q\rangle \boldsymbol{\alpha}_S \langle \mathbf{e}_Q\rangle\right\} \tag{3-21}$$

which has indeed the form of a variation.

At distances between S and Q where the charge distributions overlap the analysis of the interaction energy becomes much more complicated [27,95,100] because the total wave function must obey the Pauli principle:

$$\Psi^0_{QS} = \hat{A}^{as}_{QS}\Psi^0_Q \otimes \Psi^0_S \tag{3-22}$$

with $\hat{A}^{as}_{QS}$ the antisymmetrizing operator, generating a form of $\Delta U^{(2)}_{disp}$ that cannot be separated into fragment wave functions. Starting, e.g., from a Hartree–Fock calculation to get the total energy of the superimposed fragments, corrected for basis set superposition errors (BSSE) [101,102], the first physically meaningful interaction energy can be defined only after satisfying the Pauli principle. This is achieved by orthogonalizing the fragment wave functions, which contributes ΔU^{HF}_{orth} to the interaction energy that can therefore best be written as

$$\Delta U_{\text{int}} = U^{HF}_{Q+S} - \left(U^{HF}_Q + U^{HF}_Q\right) + \Delta U_{orth} \approx \Delta U^{(1)}_{\text{int}} + \Delta U_{rep} + \Delta U_{response} \tag{3-23}$$

Alternatively, one can calculate energies of overlapping charge distributions with symmetry-adapted perturbation theory (SAPT) [95,100], the intermolecular Møller–Plesset (I-MP) perturbation theory [27] or apply schemes as defined by Karlström et al. [36]. However, these procedures require many calculations on specific molecular aggregates which are for systems we have in mind—large (bio)molecules in various solvents—impractical. Because of this the short-range repulsion, which is formally part of $\hat{V}^{\text{response}}_S$, is modeled with ad hoc potentials which in general do not affect the electrons. Hence the QM/MM part of our approach is finding a self-consistent solution for

$$U_{Q+S} = \left\langle \Psi_Q(\mathbf{r}_q) \left| \hat{H}^0_Q(\mathbf{r}_q) + \hat{V}_S(\mathbf{r}_q) \right| \Psi_Q(\mathbf{r}_q) \right\rangle = U^0_Q + \Delta U_{\text{int}} \tag{3-24}$$

with

$$\ddot{V}_S(r_q) = \sum_{\substack{q\in Q \\ s\in S}} \frac{z_s}{|\mathbf{r}_q - \mathbf{r}_s|} + \ddot{V}^{response}_S(\boldsymbol{\alpha}_S, \mathbf{r}_q) \tag{3-25}$$

in which $\ddot{V}^{\text{response}}_S$ contains the many-body polarization and dispersion contributions to the interaction energy. Provided one has a good model for the charge distribution and the polarizability of S, $\ddot{V}^{\text{response}}_S$ can be constructed and used directly for the MM part of the system, while in the QM/MM problem it has to be expressed in terms useful in QM calculations. In the following sections we discuss the modeling of electrostatic potentials and the many-body polarization.

3.2.2. Electrostatic Potentials: The Point Charges

Electrostatic potentials and fields of classical molecules are generated by a collection of point charges—generally on atoms—obtained from QM calculations and defined such that they at least reproduce the vacuum dipole moment [103], or also the quadrupole moment [69], i.e., the first- and second-order sources of the electric field

of neutral molecules. The methods referred to are internal in the sense that no fitting to calculated potentials or fields is necessary. The first one is just an extension of the Mulliken population analysis [104], in which the overlap and dipole integrals are contracted with the density matrix (**D**) to give Mulliken atomic charges and dipoles:

$$q_A^{Mul} = Z_A - \left\{ \sum_{i,j \text{ on } A} D_{ij} \langle \chi_i | \chi_j > + \frac{1}{2} \sum_{\substack{i \text{ on } A \\ j \text{ on } B \neq A}} D_{ij} \langle \chi_i | \chi_j > \right\}$$

$$\mu_A^{Mul} = Z_A \mathbf{r}_A - \left\{ \sum_{i,j \text{ on } A} D_{ij} \langle \chi_i | \mathbf{r} | \chi_j > + \frac{1}{2} \sum_{\substack{i \text{ on } A \\ j \text{ on } B \neq A}} D_{ij} \langle \chi_i | \mathbf{r} | \chi_j > \right\} \tag{3-26}$$

with $\{\chi\}$ the basis functions in which the wave function and operators are expanded, and Z_A the atomic number of A. The next step is to redefine the atomic charges such that the total charge (Q) and the dipole moment of the molecule ($\boldsymbol{\mu}_{\text{mol}}$) are preserved:

$$\sum_A q_A = Q_{mol}; \sum_A q_A \mathbf{r}_A = \mu_{mol} \tag{3-27}$$

We note that ($\boldsymbol{\mu}_A^{Mul} - q_A^{Mul} \mathbf{r}_A$) in Eq. (3-27) is the induced (Mulliken) dipole on atom A which is 'charge free' and hence can be moved or reconstructed in any way one wishes. Additional expansion centers may be defined if required, e.g., by symmetry. Equations (3-27) can be satisfied in many ways. We choose to take the smallest possible charges, placed on the nearest atoms, compatible with Eq. (3-27). This can be achieved by minimizing

$$\sum_A q_A^2 / 2 w_A \tag{3-28}$$

with w_A a weighting function that decreases more or less rapidly with the distance relative to the position of A. Thole and van Duijnen [103] took Gaussians with interatomic distances as parameter for defining the weights. Swart et al. [70] applied the same technique—implemented so far only in the Amsterdam density functional theory (ADF) package [86]—for representing the atomic multipoles up to the quadrupole moment. These moments result directly from the numerical integrations in ADF and they obviously add up to the molecular moments. These atomic moments are used also for generating the electric potential *inside* a molecule accurately and hence are even better for generating the *external* potential. For obtaining the redistributed charges that reproduce as well as possible the total charge (Q), dipole ($\mu_{i,A}^M$) and quadrupole ($\theta_{jk,A}^M$) moment components Swart et al. [70] minimize the function

$$g_A = \sum_s \frac{q_{s,A}^2}{2w_{s,A}} + \xi_A \left(q_A^M - q_A^{repr}\right) + \sum_i \tau_{i,A} \left(\mu_{i,A}^M - \mu_{i,A}^{repr}\right) + \sum_{j,k} \eta_{jk,A} \left(\theta_{jk,A}^M - \theta_{jk,A}^{repr}\right) \cdots \tag{3-29}$$

with ξ_A, $\tau_{i,A}$ and $\eta_{jk,A}$ Lagrange multipliers, $\{i,j,k \in x,y,z\}$ and $w_{s,A}$ the weight factor defined by

$$w_{s,A} = \exp\left(\frac{-\zeta\left(|\mathbf{r}_s - \mathbf{r}_A|\right)}{d_A}\right) \tag{3-30}$$

with d_A the distance between center A and its nearest neighbor, and ζ an exponential prefactor. The redistributed charges then are

$$q_{s,A} = w_{s,A}\left(\xi_A + \sum_i \tau_{i,A} r_{sA,i} + \sum_{j,k} \eta_{jk,A}\left\{\frac{3}{2} r_{sA,j} r_{sA,k} - \frac{1}{2}\delta_{jk} r_{sA}^2\right\} + \cdots\right) \tag{3-31}$$

For each site in the set there is a set of linear equations which are solved by a standard **Ax=b** routine. The prefactor ζ in Eq. (3-30) must in principle be large for the reproduced multipoles to be as local as possible, but if it is very large the weight function approaches a delta function, leading to the loss of freedom to distribute the charges over other atoms. The 'optimal' value was chosen such as to make the errors in the represented multipoles (due to machine precision and numerical accuracy) smaller than the accuracy required for the numerical integration of some typical cases (a set of amino acid residues). The best choice turned out to be 3.0. The resulting MDC-q charges is for a number of small molecules given in Table 3-1.

These internal procedures for obtaining point charges are preferred over, e.g., potential-derived charges [105,106,107] since the latter require the definition of a grid of points where the quantum-chemical potential is fitted to the static potential of the point charges. The drawbacks are manifold: strong dependence on the size and form of the grid, the fitting method, numerical instability, etc. Furthermore, there are uncertainties in assigning charges to buried atoms, because the atoms near the grid mainly determine the potential outside of the molecule. Finally, these methods are very CPU intensive because of the many times that the inverse distance ($1/r$) between grid points and charges has to be evaluated. In contrast, the internal methods described above are almost trivial in terms of CPU costs: they take slightly more than the usual Mulliken analysis and can be done 'on the fly', e.g., inside SCF iterations whenever needed.

3.2.3. The Many-Body Polarization

For a collection of (atomic) polarizabilities in an electric field, assuming linear response, the induced dipole moment at site s is

Table 3-1. MDC-q charges for some molecules

Molecule	Charges	Molecule	Charges
Benzene		Hexafluorobenzene	
q_C	−0.123	q_C	0.094
q_H	0.123	q_F	−0.094
Ethylene		Ammonia	
q_C	−0.250	q_N	−0.444
q_H	0.125	q_H	0.148
Carbondioxide		Carbondisulfide	
q_C	0.574	q_C	−0.351
q_O	−0.287	q_S	0.185
Methylcyanide		Thiophene	
$q_{C\text{-}Me}$	0.692	q_S	0.051
q_H	−0.157	$q_{C'}$	−0.229
q_C	0.203	$q_{H'}$	0.206
q_N	−0.425	$q_{C''}$	−0.176
		$q_{H''}$	0.173

$$\mu_{s,i}^{ind} = \alpha_{s,ij}\left[e_{s,i}^{init} + \sum_{i,j} T_{st,ij}^{(2)}\mu_{t,j}^{ind}\right]; \quad i, j \in x, y, z \tag{3-32}$$

where $\alpha_{s,ij}$ is a component of the polarizability tensor at site s, which for an isotropic atom is $\alpha_{s,ij} = \delta_{ij}\alpha_s$. In Eq. (3-32) $\mathbf{e}^{\text{init}}$ is the initial field at site s and the last term is the field from the induced dipoles at the other sites. The self-consistent solution of Eq. (3-32) for all induced dipoles **M** can be written as a matrix equation:

$$\mathbf{M} = \mathbf{E}\,\mathbf{B} \tag{3-33}$$

where **B** is the relay matrix defined in supermatrix notation as

$$\mathbf{B} = \left[\mathbf{A^{-1}} - \mathbf{T^{(2)}}\right]^{-1} \tag{3-34}$$

in which $\mathbf{A^{-1}}$ is the block-diagonal matrix of the site-inverse polarizabilities, and $\mathbf{T}^{(2)}$ the off-diagonal interaction tensors, **M** the supervector of all induced dipoles in the system and **E** the vector of all initial local fields. Equation (3-33) can be solved by means of an exact inversion constructing **B** explicitly, or by iteration using $\mathbf{MB}^{-1} = \mathbf{E}$. We note that **B** in Eq. (3-33) behaves as a 'normal' (but many-center) polarizability. We note that the polarization energy is given by

$$\Delta U_{ind} = -1/2\left(\mathbf{E}^0\right)^T \mathbf{B}\mathbf{E}^o = -1/2\sum_i (\mathbf{e}_i^0)^T \boldsymbol{\mu}_i = -1/2\sum_i (\mathbf{e}_i^0)^T \boldsymbol{\alpha}_i \mathbf{e}_i \tag{3-35}$$

which, due to the self-consistency, is quadratic neither in the permanent fields $\mathbf{e}_i{}^0$nor in the total fields $\mathbf{e}_i$.

The matrix **B** can be reduced to smaller dimensions by summing over (groups of) atoms:

$$\alpha_{ij}^G = \sum_{p,q}^{N^G} (B_{pq})_{ij}\,; i, j \in \{x, y, z\} \tag{3-36}$$

resulting in a 3×3 *molecular* polarization if the summation comprises all the atoms in the group.

The polarizabilities parallel ($\alpha_{//}$) and perpendicular ($\alpha_{\perp}$) to the axis connecting two interacting atoms p and q—are given by Silberstein's equations [58] which are the exact solutions of Eq. (3-34):

$$\alpha_{//} = \frac{\alpha_p + \alpha_q + 4\alpha_p\alpha_q/r^3}{1 - 4\alpha_p\alpha_q/r^6}; \alpha_{\perp} = \frac{\alpha_p + \alpha_q - 2\alpha_p\alpha_q/r^3}{1 - \alpha_p\alpha_q/r^6} \tag{3-37}$$

Even for the case of isotropic polarizabilities, where $\alpha_p = \alpha_q = \bar{\alpha}$, it follows from Eq. (3-36) that the total polarizability will be anisotropic. If we want to define *effective* polarizabilities from Eq. (3-37) for the members, we must (arbitrarily!) distribute the interaction term. For $\alpha_p = \alpha_q$ equipartitioning could work, leading to local anisotropy with $\alpha_{//}$ (local)>$\bar{\alpha}$ and $\alpha_{\perp}$ (local)<$\bar{\alpha}$, but for $\alpha_p \neq \alpha_q$ no scheme is obvious.

One possibility is weighting the partitioning with the original polarizabilities [108]. This may work better in the general case, but it is just as arbitrary. What will happen to local (anisotropic) polarizabilities in the condensed phases is hard to estimate without calculations. Some typical model systems can be found in Ref. [24]. It is also demonstrated by the work of Augspurger and Dykstra [109] on acetylene clusters where for *linear* complexes an *increase* of the axial components of the linear and second hyperpolarizabilities are found, while van Duijnen et al. [110] for *parallel* clusters of butadienes and Kirtman et al. [111] for hexatrienes obtained a *decrease* in the same properties. These authors also show that well-constructed fully classical electrostatic models are able to reproduce these results.

Here we note that only a single polarizability or susceptibility exists for any system. The reconstruction from local contributions is in fact an abstraction, the result of which depends on the detail wanted: macroscopic with local susceptibilities or microscopic with local polarizabilities and—more importantly—on the partitioning of such properties. However, experimental chemists are used to such procedures: from well-chosen series of compounds they derive 'bond energies' as 'local' contributions to heats of formation and 'ionic radii' from crystal structures. Theoretical chemists obtain 'atomic charges' from, e.g., a Mulliken analysis of their wave functions. We are able, following similar reasoning, to construct molecular polarizabilities from atomic ones [38,60], although there is formally no connection between them. In an opposite direction we can 'decompose' a molecular polarizability into a many-center

matrix of effective local contributions, in which a one-to-one assignment of the interaction blocks to the corresponding diagonal 'local' blocks looks like the Mulliken scheme. A weighted assignment, e.g., with the traces of the diagonal blocks [108], will look like the Löwdin scheme for a population analysis. In this sense we can at least assess the local contributions to the system's polarizability, although only within an arbitrary but well-defined framework.

From Eq. (3-36) we learn that for r approaching $(4\alpha_p\alpha_q)^{1/6}$, $\alpha_{//}$ goes to infinity and becomes negative for smaller distances. In order to avoid this unphysical situation, Thole [59] introduced a damping scheme by rewriting the interaction tensor in terms of a reduced distance $u_{pq}=R_{pq}/(\alpha_p\alpha_q)^{1/6}$ as

$$T^{(2)}_{pq,ij} = (\alpha_p\alpha_q)^{1/2}\frac{\partial^2\phi(u_{pq})}{\partial u_{pq,i}\partial u_{pq,j}} \tag{3-38}$$

with $\Phi(u)$ the potential of a point charge at u.

The screened dipole interaction tensor (taking $\mathbf{r} = \mathbf{R}_{pq}$ for clarity) then becomes

$$T^{(2)}_{pq,ij} = \frac{3f_T r_i r_j}{r^5} - \frac{f_E r_i \delta_{ij}}{r^2} \tag{3-39}$$

with f_T and f_E damping functions depending on the particular form of ρ. Thole tried a number of forms for ρ, but in practice only an exponentially decaying charge distribution

$$\rho(u) = \frac{a^3}{8\pi}\exp(-au) \tag{3-40}$$

survived, with a the screening length. The following expressions define consistently the damped potential, field, field gradient and gradient-of-the-gradient of a point charge:

$$\begin{aligned}
v &= au \\
V &= f_V/r;\ f_V = 1 - \left(\frac{1}{2}v + 1\right)e^{-v} \\
E_i &= f_E r_i/r^3;\ f_E = f_V - \left(\frac{1}{2}v^2 + \frac{1}{2}v\right)e^{-v} \\
T_{ij} &= \frac{3r_i r_j f_T - \delta_{ij} r^2 f_E}{r^5};\ f_T = f_E - \frac{1}{6}v^3 e^{-v} \\
D_{ijk} &= \frac{3r^2(r_i\delta_{jk} + r_j\delta_{ik} + r_k\delta_{ij})f_T - 15 r_i r_j r_k f_D}{r^7}; \\
f_D &= f_T - \frac{1}{30}v^4 e^{-v}
\end{aligned} \tag{3-41}$$

With this method, Thole fitted isotropic model polarizabilities for H, C, N and O to 16 experimental molecular polarizabilities, using a single screening length and only one polarizability for each atom type, regardless of the chemical environment.

With the parameters thus obtained, the polarizabilities of six other molecules—not in the training set—containing these atoms were calculated within experimental accuracy. Van Duijnen and Swart [60] re-parameterized the same atomic polarizabilities using restricted Hartree–Fock (RHF)-optimized geometries, extended the training set to 52 molecules, the control set to 18 molecules and the set of atoms with sulfur and the halogens. Also computed molecular polarizabilities were parameterized for enabling comparison with fully quantum-chemical calculations.

The resulting atom polarizabilities fitted to experiment are summarized in Table 3-2 together with numerical Hartree–Fock results for the free atoms [112].

Comparing the fitted values with the HF results it appears that the former have more physical contents than one can expect from mere fitting parameters. The differences with the HF values are obviously related to the fact that the fitted values hold for atoms bound in molecules, which is conspicuous for H with its short bond lengths, and for C, which is in most compounds bonded to (up to four) other atoms. In Table 3-3 the polarizabilities of the control set (resulting from the fit to 52 experimental values) are listed.

In appraising the average accuracy one must bear in mind that experimentally the mean polarizabilities are usually obtained from the refractive index n (at 5893 Å, the sodium D-line) and the Lorenz–Lorentz equation (with M molecular weight, ρ macroscopic density, N_{av} Avogadro's number):

$$\frac{n^2-1}{n^2+2}\frac{M}{\rho} = \frac{4\pi}{3}N_{av}\bar{\alpha} \tag{3-42}$$

Table 3-2. Effective atomic polarizabilities (Bohr^3) from various fits

Atom	Fit to 16 molecules		Fit to 52 molecules[a]	
	Thole[b]	Geom. optimized[a]		Num. HF[c]
H	2.8815	3.0588	2.7927	4.52[d]
C	8.6716	8.7939	8.6959	11.7
N	6.5256	6.6704	6.5565	6.75
O	5.3042	5.6480	5.7494	4.93
F	–	–	3.0013	3.58
S	–	–	16.6984	23.2
Cl	–	–	16.1979	17.6
Br	–	–	23.5714	25.6
I	–	–	36.9880	42.6
a	2.089	1.9088	2.1304	–

Data from: [a]Ref. [60], [b]Ref. [59], [c]Ref. [112], [d]exact.

Table 3-3. Experimental and calculated polarizabilities for compounds *not* in the 52-membered training set of molecules[a]

Molecule		Exp	Calculated	Dev (%)
Cyclohexanol	$C_6H_{11}OH$	78.01	77.97	0.0
Dodecane	$C_{12}H_{26}$	153.86	157.76	2.4
Neopentane	$C(CH_3)_4$	68.83	65.49	4.8
Acetylene	C_2H_2	23.55	21.90	8.3
m-Dichlorobenzene	$C_6H_4Cl_2$	96.03	89.65	6.6
o-Dichlorobenzene	$C_6H_4Cl_2$	95.62	89.03	6.9
N, *N*-dimethylformamide	$HCON(CH_3)_2$	52.70	51.77	1.8
N-methylacetamide	$CH_3CONHCH_3$	52.77	51.95	1.8
Carbonylchloride	$COCl_2$	45.75	44.30	3.2
Chloromethylcyanide	CH_2ClCN	41.16	42.87	4.2
Isopropylcyanide	$(CH_3)_2CHCN$	54.32	54.54	0.4
Trichloromethylcanide	CCl_3CN	70.32	69.56	1.1
Dichloromethane	CH_2Cl_2	46.02	43.55	5.4
Difluoromethane	CH_2F_2	18.42	18.56	0.8
Tribromomethane	$CHBr_3$	79.90	75.99	3.8
Trichlorofluoromethane	$CFCl_3$	55.61	56.45	1.5
Triiodomethane	CHI_3	121.74	111.74	8.2
Nitrous oxide	N_2O	20.24	17.81	12.0
			Average	4.0

[a]Data from Ref. [60].

This equation is accurate in the gas phase but the refractive index should first be extrapolated to infinite wavelength (or zero frequency) to obtain the static polarizability:

$$n(\lambda) = n_{\infty}^{*} + \frac{a}{\lambda^2} + \frac{b}{\lambda^4} + \cdots \tag{3-43}$$

The polarizabilities decrease in this extrapolation by about 2–4% [113] which gives an estimate of the uncertainty in the experimental values. From Kerr constants [113] for small, symmetric molecules also the anisotropy and the frequency dependence can be determined, but the assumptions about the geometry add an uncertainty of 5–10%, giving a total uncertainty of 6–14%. Hence, an average deviation of 4% in Table 3-3 is considered to be within experimental error. From this table we also learn that the effective atomic polarizabilities work fine within Thole's model for predicting polarizabilities of virtually any system comprising these atoms. If no experimental data are available, one may predict molecular polarizabilities. In Table 3-4 polarizabilities of various molecules are collected as obtained from different computational approaches together with the experimental values. Calculation of polarizabilities is based on a Taylor expansion of the total energy (or the dipole moment) of a system in an external field:

Table 3-4. Some experimental and calculated molecular polarizabilities[a]

Molecule	α_{exp}	α_{DRF}	α_{CPHF}(TZP)	α_{DFT}(TZ2P++)
Acetamide	40.5	38.6	31.1	43.1
Acetylene	22.4	21.9	18.0	23.1
Benzene	70.1	61.9	61.9	72.6
Chlorine	31.1	31.2	18.7	31.7
Cyclohexane	80.0	78.0	69.2	82.7
Dimethylether	79.9	35.4	27.6	36.3
Formaldehyde	16.5	18.3	13.5	18.3
Hydrogen	5.33	4.90	2.62	5.76
Methylcyanide	29.7	29.8	24.6	31.1
Neopentane	69.0	655	59.0	1.3
Propane	42.4	42.2	35.9	44.1
TCFM	57.5	56.5	40.0	60.9
TCMC	70.5	68.3	54.0	75.2
TFM	19.0	19.0	13.1	18.9
Water	9.94	10.1	5.56	9.38
Deviation	–	±4.8%	±12%	±3%
Time	–	< 1 s	57 h	80 h

[a]Data from Ref. [60].

$$U = U^{(0)} - \mu_i^{(0)} e_i - \frac{1}{2!}\alpha_{ij} e_i e_j - \frac{1}{3!}\beta_{ijk} e_i e_j e_k - \frac{1}{4!}\gamma_{ijkl} e_i e_j e_k e_l$$

or

$$\mu_i = \mu_i^{(0)} e_i - \alpha_{ij} e_j - \frac{1}{2!}\beta_{ijk} e_j e_k - \frac{1}{3!}\gamma_{ijkl} e_j e_k e_l; \; i, j, k, l \in \{x, y, z\} \tag{3-44}$$

with $U^{(0)}$the unperturbed total energy, $\mu^{(0)}$ the permanent dipole moment and α, β and γ the linear polarizability and the first and second hyperpolarizabilities. For molecules with closed-shell ground states the coupled perturbative Hartree–Fock (CPHF) equations [83] can be used. However, RHF results give an average difference with experiment of about 25% for small- to medium-sized basis sets [60]. It is known that specially constructed [114,115,116] or very large basis sets (including very diffuse functions) [117] are needed, in particular for planar and linear molecules. Furthermore, taking electron correlation into account is essential in order to get results comparable with the experimental values. Configuration interaction (CI), multi-configuration SCF (MCSCF), coupled cluster (CC) or Møller–Plesset (MP) methods, combined with the required large basis sets, are computationally very demanding. Promising and accurate are density functional theory (DFT) results. Depending on the exchange–correlation (XC) potentials and the basis set, a deviation of 3% can be obtained, which is about the experimental accuracy, although DFT

polarizabilities of conjugated systems [118,119] and systems with large charge transfer character [120,121] tend to be too large. Table 3-4 is clear: one has to spend a fair amount of computing time by doing high-quality QM calculations for gaining about 0.6% accuracy for relatively small molecules. For large (bio-)organic molecules QM calculations of this quality are obviously beyond practical possibilities and therefore methods like Thole's are the best approach.

There are other parameterizations possible. Thole noted, in his original paper, that it would be more elegant to describe the interaction—between induced dipoles—in terms of two interacting charge distributions instead of his 'one-particle' ansatz. Jensen et al. [35] took up this suggestion in order to arrive at traceless interaction tensors. He started from the interaction between two isotropic Gaussian charge distributions on a distance r:

$$V = \int\int \frac{\rho(r_1)\rho(r_2)}{r_{12}} \mathrm{d}r_1 \mathrm{d}r_2 = \frac{\mathrm{erf}(\mathrm{r}\sqrt{\mathrm{b}})}{r} \tag{3-45}$$

Here is b the reduced exponent $b = a_p\, a_q \,/\, (a_p + a_q)$ and erf $\left(r\sqrt{b}\right)$ the regular error function which tends to unity when the argument goes to infinity, and hence the usual potential between two point charges is obtained. The results with the Gaussians are only slightly better [66] than that of Thole's original method. Another approach is that of Pircaud et al. [122] who start from partial charges for water reproducing the vacuum dipole moment that are 'inflated' by Gaussians and used together with the experimental polarizability. This amounts to the use of the screened potential of Eq. (3-41).

Concluding this section, we are confident that the present treatment of the many-body polarization gives transferable and reliable effective polarizabilities and screening factors.

3.2.4. Bulk Effects: The Dielectric Continuum

The collective properties of bulk material typically reflect the behavior of tens of thousands of molecules in a volume of at least 10^6 Å^3 [123]. The description of the electrostatic and response properties of such volumes is obviously beyond any discrete approach and one has to resort to experimental information, i.e., the dielectric constant. In the Introduction we argued that if sufficient solvation shells are included in a calculation, the effect of an enveloping continuum can be neglected. Nevertheless we give here, for completeness' sake, an explicit formulation of the coupling between a set of point charges and polarizabilities and a dielectric continuum.

The extension of Eq. (3-32) is straightforward: for a discretized enveloping surface (**S**) with the boundary element method (BEM) the final result can be expressed in a set of linear equations [124]:

$$\begin{bmatrix} \mathbf{M}_p \\ \mathbf{\Omega}_I \end{bmatrix} = \mathbf{B}' \begin{bmatrix} \mathbf{e}_p \\ \hline \dfrac{\mathbf{v}_I}{2\pi(\varepsilon+1)} \end{bmatrix} \tag{3-46}$$

where in the lhs vector **M** represents the induced dipoles at the polarizable points and **Ω** a set of induced dipoles on the surface **S**. In the rhs **e** and **v** are, respectively, the source fields at the polarizable points and the potentials at the N^{BEM} representative points of **S**. The matrix $\mathbf{B}'$ is given by

$$\mathbf{B}' = \begin{bmatrix} \boldsymbol{\alpha}_p^{-1} - \mathbf{T}_{pq}^{(2)} & \nabla \mathbf{K}_{Ip} S_I \\ \dfrac{-\mathbf{e}_{pI}}{2\pi(\varepsilon+1)} & \mathbf{1} - \dfrac{\mathbf{K}_{IJ}}{2\pi(\varepsilon+1)} \end{bmatrix}^{-1} \tag{3-47}$$

with ε the dielectric constant of the continuum. In Eqs. (3-46) and (3-47) we have added (redundant) indices for clarity: lower case indices for discrete polarizable points and capitals for boundary elements. In the top left of Eq. (3-47) the matrix of Eq. (3-34) will be recognized, while **K** and ∇**K** are more or less complicated potential and field-like kernels, depending on ε and the geometry of **S,**while **1** is the unit matrix of dimension N^{BEM} [10,124]. Hence, leaving out the continuum Eq. (3-34) alone remains, while for the continuum only, just the right bottom part of Eq. (3-47) remains and we are left with a method like the polarizable continuum model (PCM) [9,17]. Like **M** in Eq. (3-33) the lhs of Eq. (3-46) is a self-consistent solution and all information about the reaction potentials is contained in a single relay matrix.

3.2.5. Implementations

In the preceding sections, we have shown that our point charges and polarizabilities can generate trustworthy electrostatic and response properties for any system. The working expression for the DRF/QM/MM method is

$$\hat{H}(r) = \hat{H}_{QM} + \hat{H}_{QM/MM} + \hat{H}_{MM} \tag{3-48}$$

The interaction operator at any point $\mathbf{r}_\mathrm{i}$ is given by

$$\begin{aligned} \hat{H}_{QM/MM}(\mathbf{r}_i) = \sum_i \hat{v}^{DRF}(\mathbf{r}_i, \omega) = \sum_i \hat{v}^{elst}(\mathbf{r}_i) \\ + \sum_i \hat{v}^{pol}(\mathbf{r}_i, \omega) + \left[\sum_i \hat{v}^{disp}(\mathbf{r}_i) \right] \end{aligned} \tag{3-49}$$

where v^{elst} is the electrostatic operator, which describes the Coulombic interaction between the QM system and the permanent charge distribution of the solvent molecules. The polarization operator describes the many-body polarization of the solvent molecules, i.e., the change in the charge distribution of the solvent molecules due to interaction with the QM part and other solvent molecules. The dispersion operator v^{disp} is bracketed in Eq. (3-47) because it may optionally be made part of $H_{\mathrm{QM/MM}}$ or not.

The charge distribution of the solvent is represented by the atomic point charges (z_s), hence the electrostatic operator is given by

$$\hat{v}^{elst}(\mathbf{r}_i) = \sum_s \frac{z_s}{R_{si}} = \sum_s z_s \hat{T}^{(0)}_{si} \tag{3-50}$$

with R_{si} the distance between points s and i, and $T^{(0)}$ the zeroth order interaction of Eq. (3-12). Depending on the particular QM method the operator $\hat{v}^{elst}$ for the electrostatic interaction energy

$$\Delta U^{elst} = \int \rho(r_i)\hat{v}^{elst}(\mathbf{r}_i)\mathrm{d}\mathbf{r}_i \tag{3-51}$$

has to be evaluated, e.g., in ADF [86] in all integration points, or leads to additional 'nuclear attraction'-type integrals in conventional wave function methods where the operators are expanded in basis functions $\{\chi\}$:

$$\left(v^{elst}\right)_{kl} = \sum_s \int \chi_k(r_i)\frac{f_V z_s}{|\mathbf{r}_i - \mathbf{r}_s|}\chi_l(r_i)\mathrm{d}\mathbf{r}_i = \sum_s <\chi_k|\frac{f_V z_s}{R_{si}}|\chi_l> \tag{3-52}$$

The atom pairs determining the screening factor f_V of Eq. (3-52) are taken as the atoms at $\mathbf{r}_s$ and the atom(s) on which χ_k and χ_l are centered. In ADF the screening is achieved by scaling the distance between grid points and classical atoms R_{pq}:

$$S_{pq} = c_{pq} R_{pq} = f(R_{pq}) \tag{3-53}$$

where c_{pq} is a factor and $f(R_{pq})$ an appropriately chosen function of R_{pq}. Furthermore, each component of R_{pq} is also scaled by c_{pq}, so the reduced distance becomes

$$S_{pq} = \sqrt{S_{pq,\kappa} S_{pq,\kappa}} = c_{pq}\sqrt{R_{pq,\kappa} R_{pq,\kappa}} = c_{pq} R_{pq}; \kappa \in \{\mathrm{x}, \mathrm{y}, \mathrm{z}\} \tag{3-54}$$

i.e., consistent with the definition in Eq. (3-53). For Greek indices the Einstein summation convention is employed. The damped operator can thus be obtained by modifying the interaction tensors in Eqs. (3-19), which is equivalent to replacing R_{pq} by S_{pq} and $R_{ij,\kappa}$ by $S_{ij,\kappa}$ in the regular formulae for the interaction tensors:

$$T^{(n)}_{pq,\eta_1,\eta_2,\ldots,\eta_n} = \nabla_{yx,\eta_1} \ldots \nabla_{yx,\eta_n}\left(1/S_{pq}\right) \tag{3-55}$$

The particular form of the scaling function employed here is

$$f(r_{pq}) = \frac{r_{pq}}{\mathrm{erf}(r_{pq})} \tag{3-56}$$

which was obtained by considering the interaction between two Gaussian charge distributions with unit exponents. The damping ensures that the quantum part is not overpolarized due to the interactions.

The damping depends on the width of the Gaussian charge distribution, which in this work was taken to be unit (a.u.). However, both a slightly smaller width [125] and a slightly larger width [126] have been suggested.

For $\hat{v}^{pol}$ a similar route is followed:

$$\hat{v}^{pol}(r_i, \omega) = -\sum_s \mu_s^{ind}(\omega)\mathbf{T}_{si}^{(1)} \tag{3-57}$$

with $\boldsymbol{\mu}_s^{\mathrm{ind}}(\omega)$ the induced dipole moment at atom s, obtained from Eqs. (3-33) and (3-34):

$$\mathbf{M}(\omega) = \mathbf{E}^{\mathrm{init}}(\omega)\mathbf{B} \tag{3-58}$$

The initial field consists of four terms:

$$\mathbf{e}_s^{\mathrm{init}}(\omega) = \mathbf{e}_s^{\mathrm{QM,el}}(\omega) + \mathbf{e}_s^{\mathrm{QM,nuc}} + \mathbf{e}_s^{\mathrm{MM}} + \mathbf{e}_s^{\mathrm{mac}}(\omega) \tag{3-59}$$

where $\mathbf{e}_s^{\mathrm{QM,el}}(\omega)$ is the electric field arising from the electronic charge distribution of the QM part:

$$\mathbf{e}_s^{\mathrm{QM,el}}(\omega) = -\int \rho(\mathbf{r}_i, \omega)\mathbf{T}_{si}^{(1)}\mathrm{d}\mathbf{r}_i \tag{3-60}$$

and $\mathbf{e}_s^{\mathrm{QM,nuc}}$ is the field arising from the QM nuclei,

$$\mathbf{e}_s^{\mathrm{QM,nuc}} = -\sum_n Z_n \mathbf{T}_{ns}^{(1)} \tag{3-61}$$

and $\mathbf{e}_s^{\mathrm{MM}}$ is the field arising from the point charges of the solvent molecules,

$$\mathbf{e}_s^{\mathrm{MM}} = -\sum_t{}' q_s \mathbf{T}_{st}^{(1)} \tag{3-62}$$

The prime in Eq. (3-62) indicates that the sum is restricted to sites that do not belong to the same molecule. Depending on the specific implementation the tensors $\mathbf{T}^{(1)}$ are multiplied with appropriate f_E factors for the associated atoms. The last term in Eq. (3-59), $\mathbf{e}_s^{\mathrm{mac}}(\omega)$, is the macroscopic electric field. This completes the most usual form of $\hat{v}^{pol}$, i.e., the potential of the dipoles due to the total field at the polarizable sites is made a part of the effective Hamiltonian and Eq.(3-24) is solved self-consistently. Since the induced dipoles $\mathbf{M}$ in the solvent (MM) part are self-consistent for any field $\mathbf{E}$, i.e., also for intermediate fields during the iterative process for solving Eq. (3-24), in this way we obtain an overall self-consistent solution, similar to, e.g., the HF or Kohn–Sham procedure. Extension to post-HF methods are straightforward because the reaction potential (RP) is formally a one-particle

operator and in, e.g., the configuration interaction (CI) method only the diagonal CI-matrix elements are affected which can be evaluated by calculating $\mathbf{e}_s^{\mathrm{QM,el}}$ for the various determinants. The final CI states thus obtained are not strictly self-consistent but for a small number of solutions one may recalculate the RP and reiterate.

The electronic contribution to ΔU^{int} is $\Delta U_{el}^{\mathrm{int}} = -1/2\,(\mathbf{E}^{QM,el})\,\mathbf{B}\mathbf{E}^{QM,el}$ and in its earliest form of DRF (the *direct* reaction field approach [3,38]) v^{DRF} was of the form

$$\ddot{v}^{pol} = -1/2 \sum_{i,j} \ddot{\mathbf{E}}_i \mathbf{B} \ddot{\mathbf{E}}_j \tag{3-63}$$

where the summation runs over all particles in QM. If i or j is related with an electron, the integral of Eq. (3-52) appears naturally, but in addition integrals for the *screened self-interaction* appears:

$$I_{km}^{self} = -\frac{1}{2} \int\int \chi_k(\mathbf{r}_1) \left[\ddot{\mathbf{T}}^{(1)}(\mathbf{r}_1) \mathbf{B} \ddot{\mathbf{T}}^{(1)}(\mathbf{r}_1) \right] \chi_m(\mathbf{r}_1) \mathrm{d}\mathbf{r}_1 \tag{3-64}$$

and, if i and j both refer to electrons, screened 2-electron integrals are

$$\begin{aligned} I_{klmn}^{two} &= -\frac{1}{2} \int\int \chi_k(\mathbf{r}_1)\chi_l(\mathbf{r}_2) \ddot{\mathbf{T}}^{(1)}(\mathbf{r}_1) \mathbf{B} \ddot{\mathbf{T}}^{(1)}(\mathbf{r}_2) \chi_m(\mathbf{r}_1)\chi_n(\mathbf{r}_2) \mathrm{d}\mathbf{r}_1 \mathrm{d}\mathbf{r}_2 \\ &= -\frac{1}{2} \left\{ \int \chi_k(\mathbf{r}_1) \ddot{\mathbf{T}}^{(1)}(\mathbf{r}_1) \chi_m(\mathbf{r}_1) \mathrm{d}\mathbf{r}_1 \right\} \times \left\{ \int \chi_l(\mathbf{r}_2) \mathbf{B} \ddot{\mathbf{T}}^{(1)}(\mathbf{r}_2) \chi_n(\mathbf{r}_2) \mathrm{d}\mathbf{r}_2 \right\} \end{aligned} \tag{3-65}$$

They may be added to the standard integrals used in, e.g., a standard HF calculation and, after contracting the integrals in Eq. (3-65) with the density matrix, this gives the following contributions to the energy in terms of MOs:

$$<\mathrm{self}> = -\frac{1}{2} \sum_{K_{\mathrm{occ}}} <K \left| \left[\mathbf{T}^{(1)}(\mathbf{r}_1) \mathbf{B} \mathbf{T}^{(1)}(\mathbf{r}_1) \right] \right| K> \tag{3-66}$$

and

$$\begin{aligned} <\mathrm{scoul}> &= a \sum_{K,L=1,n_{\mathrm{occ}}} -\frac{1}{2} <K(1)L(2) \left| \frac{1}{2} \left[\mathbf{T}^{(1)}(\mathbf{r}_1) \mathbf{B} \mathbf{T}^{(1)}(\mathbf{r}_2) \right] \right| K(1)L(2)> \\ <\mathrm{sexch}> &= -b \sum_{K,L=1,n_{\mathrm{occ}}} -\frac{1}{2} <K(1)L(2) \left| \frac{1}{2} \left[\mathbf{T}^{(1)}(\mathbf{r}_1) \mathbf{B} \mathbf{T}^{(1)}(\mathbf{r}_2) \right] \right| K(2)L(1)> \end{aligned} \tag{3-67}$$

where $a/b = 2.0$ for a closed-shell determinant but varies for open shells. It is clear that <scoul> is just the electronic reaction field contribution obtained above. The

presence of <sexch>, missing in the molecular field approach from which we started above, is correct because it removes energy contributions that violate the Pauli principle. The new one is <self> that describes the stabilization of an electron in its own reaction field . The operator in Eq. (3-64) can always be rewritten as

$$\left[\hat{\mathbf{T}}(\mathbf{r}_1)\hat{\mathbf{BT}}(\mathbf{r}_1)\right] = \hat{\mathbf{G}}^2(\mathbf{r}_1) \tag{3-68}$$

and by applying the closure rule we obtain

$$\begin{aligned}\langle \text{self}\rangle &= -\frac{1}{2}\sum_{K=1,\text{nocc}} \left\langle K\left|\left[G^2(\mathbf{r}_1)\right]\right|K\right\rangle \\ &= -\frac{1}{2}\sum_{\substack{K=1,\text{nocc}\\ L=1,\infty}} \langle K|\left[G(\mathbf{r}_1)\right]|L\rangle\,\langle L|\left[G(\mathbf{r}_1)\right]|K\rangle\end{aligned} \tag{3-69}$$

so that in the total energy the sum of the screened self-energy and the exchange becomes

$$\langle \text{self}\rangle + \langle \text{sexch}\rangle = -\frac{1}{2}\sum_{\substack{K=1,\text{nocc}\\ L=\text{nocc}+1,\infty}} \langle K|G(\mathbf{r})_1|L\rangle\langle L|G(\mathbf{r})_1|K\rangle \tag{3-70}$$

We note that **G** is associated with the polarizability of the classical system, for which we may write $\boldsymbol{\alpha} = \frac{|\langle 0|\mathbf{r}|n\rangle|^2}{U^{(0)}-U^{(n)}}$, i.e., a sum of matrix elements connecting singly excited states. In Eq. (3-70) we see similar matrix elements connecting ground state and singly excited states of the quantum system, and hence formally the self-consistent result there is a representation of second-order terms of perturbation theory (cf. Eq. 3-16) up to third order. However, in Eq. (3-70) the energy denominators are absent and, hence, this is only an upper bound for the dispersion. Moreover, integrals that appear in ⟨self⟩ are divergent: the quadratic operator is of type $f(r)/r^4$, with r the distance between a source and a polarizability, while the integrating volume is only $\sim r^3$. There are several methods to cure this problem. In one the reaction field is expanded, e.g., to second order, so that all integrals can be expressed in combinations of overlap and dipole integrals [3,10,38]. In another, a small region around the center of the polarizabilities is excluded [127]. In order to repair the absence of the energy denominators of the QM part of the system in Eq. (3-70) we use the factor

$$\gamma = \frac{U_S}{U_Q + U_S} \tag{3-71}$$

with U_S and U_Q the experimental or computed ionization energies, respectively, to arrive at a London-like ground state dispersion energy:

$$\Delta U_{\text{int}}^{\text{two-el}} = \langle \text{scoul}\rangle + \gamma\,\{\langle \text{self}\rangle + \langle \text{sexch}\rangle\} \tag{3-72}$$

If $\gamma = 0$, the procedure is equivalent to the molecular or *average* reaction field (ARF) according to Eq. (3-57).

The direct approach looks at first sight complicated, but it is in fact very efficient because by incorporating reaction field integrals in the standard set of integrals no 'external' cycles for computing fields, etc., are necessary: the whole process described in Eq. (3-52) is gone through once to obtain the necessary integrals and afterward the programs do not know the difference. The direct reaction field operator can always be used *after* an ARF calculation in order to get an estimate of the dispersion. The *direct* and *average* methods are available in HONDO [83], ZINDO [84] and GAMESS [85] while in ADF [86] only ARF is possible.

The MM Hamiltonian contains obviously the same $\hat{v}^{elst}$ and $\hat{v}^{pol}$ but acting on classical sites:

$$\hat{v}^{elst}(\mathbf{r}_p) = \sum_s{}' \frac{z_s}{R_{sp}} f_{V_{sp}} = \sum_s{}' z_s f_{V,sp} \hat{T}^{(0)}_{sp} \tag{3-73}$$

$$\hat{v}^{pol}(\mathbf{r}_p, \omega) = -\sum_s{}' \mu^{ind}_s(\omega) f_{E,sp} \mathbf{T}^{(1)}_{sp} \tag{3-74}$$

where the prime indicates that interactions between sites belonging to the same molecule or group are excluded.

For the classical dispersion interaction we use the Slater–Kirkwood expression of Eq. (3-20):

$$\Delta U^{disp}_{sp} = -\frac{1}{4} \frac{\mathrm{Trace}[\boldsymbol{\alpha}_p \mathbf{T}^{(2)}_{sp} \mathbf{T}^{(2)}_{sp} \boldsymbol{\alpha}_p]}{\sqrt{\alpha_s/n_s} + \sqrt{\alpha_p/n_s}} \tag{3-75}$$

with α the average polarizability. This interaction can be between two atomic or group polarizabilities, which may be treated as isotropic or anisotropic. In the isotropic case, Eq. (3-75) reduces to a simpler form:

$$\Delta U^{disp}_{sp} = -\frac{6}{4} \frac{\alpha_s \alpha_p}{\sqrt{\alpha_s/n_s} + \sqrt{\alpha_p/n_s}} \frac{\frac{3}{2} f^2_{T,sp} - f_{T,sp} f_{E,sp} - \frac{1}{2} f^2_{E,sp}}{R^6_{sp}} \tag{3-76}$$

while in the anisotropic case the expression is slightly more complicated [87].

The expression for the short-range repulsion is closely connected to Eq. (3-75):

$$\Delta U^{rep}_{sp} = -\frac{1}{2} \Delta U^{disp}_{sp} \frac{\left(R_{vdw,s} + R_{vdw,p}\right)^6}{R^6_{sp}} \tag{3-77}$$

that can be taken either as isotropic or anisotropic. Furthermore, the dispersion term within Eq. (3-77) may include screening factors that account for overlapping charge

densities (consistent with Eqs. (2.4.28) and (2.4.29)), or without these factors as done typically in standard force fields such as CHARMM, and our early work).

When taken together with dispersion, the short-range repulsion is thus modeled by the Lennard-Jones potential:

$$U_{\mathrm{LJ}} = D_0 \left[\rho^{-12} - 2\rho^{-6}\right] \tag{3-78}$$

with $\rho = r/R_0$. In this representation, the potential has a minimum with well depth D_0 and equilibrium distance R_0 ($\rho = 1$). It can easily be transformed into an X6-form, which uses a more realistic exponential short-range repulsion:

$$U_{\mathrm{X6}} = D_0 \left[\frac{6}{\zeta - 6} e^{\zeta(1-\rho)} - \frac{\zeta}{\zeta - 6} \rho^{-6} \right] \tag{3-79}$$

By choosing a value of ζ=12, the long-range dispersion does not change with respect to the LJ formula of (3-78), while a value of ζ = 13.772 results in a second derivative at the equilibrium distance R_0 that is equal to the LJ value ($72 \cdot D_0$). Hence, the latter value (13.772) does not change the shape of the energy curve around the equilibrium and is therefore chosen as default in DRF90 [87], since we are interested in the condensed phase, i.e., the region around the equilibrium. Note that the well depth and equilibrium distance are equal to that of the LJ form, irrespective of the choice for ζ.

For the atomic radii needed in Eq. (2.4.30), there exist many options but the default in DRF90 [87] is to use charge-dependent atomic radii using Frecer's model [128] in which a polynomial of third order is used to describe the change in atomic radii due to the atomic charge. If the atomic charge is positive, it means that less electrons are surrounding this atom, and therefore the radius is smaller. When negative, the radius increases following the same reasoning.

Both dispersion and repulsion contributions—although basically belonging to $\hat{H}_{MM}$—should of course be added to the QM/MM interactions when doing QM/MM geometry optimizations or MD simulations, using the same parameters for the QM atoms. However, in single-point energy calculations they add only to the total energy since the operators do not affect the electrons. Since the effective atomic charges can be obtained 'on the fly' during any QM calculation it is possible to let them have influence on the results, e.g., in calculations of spectra (if total energies are used) or in structure optimizations.

For MD and/or QM/MM geometry optimizations gradients of the energies are needed. They follow naturally from the energy expressions by replacing electrostatic potential and field operators by, respectively, the corresponding field and field gradient operators.

3.2.6. Macroscopic and Microscopic Properties

It is obviously useful to compare calculated and experimental values for response properties like (frequency-dependent) polarizabilities α, and hyperpolarizabilities β

and γ. This comparison is not without problems—in particular for β and γ—because of the many different conventions and experimental techniques that are used [129]. The linear polarizabilities, α, are experimentally usually obtained from refractive indices applying the Lorenz–Lorentz equation (3-42). For the hyperpolarizabilities different conventions used in calculations and experiments can lead to differences up to 300%, and that apart from different references used experimentally. All this can be avoided by clearly stating the convention used. In a macroscopic electric field

$$F_J^{mac}(t) = F_{0,J}^{mac} + F_{\omega,J}^{mac}\cos(\omega t) \tag{3-80}$$

the polarization, i.e., the dipoles averaged over a macroscopic volume, is usually expressed as a power series in the field strength:

$$\begin{aligned} P_I^{\omega_s} = {} & \delta_{\omega_s,0}P_I^0 + \chi_{IJ}^{(1)}(-\omega_s;\omega_s)F_{\omega_s,J}^{mac} \\ & + C(-\omega_s;\omega_a,\omega_b)\chi_{IJK}^{(2)}(-\omega_s;\omega_a,\omega_b)F_{\omega_a,J}^{mac}F_{\omega_b,K}^{mac} \\ & + C(-\omega_s;\omega_a,\omega_b,\omega_b)\chi_{IJKL}^{(3)}(-\omega_s;-\omega_s;\omega_a,\omega_b,\omega_b)F_{\omega_a,J}^{mac}F_{\omega_b,K}^{mac}F_{\omega_c,L}^{mac} \end{aligned} \tag{3-81}$$

where the output frequency $\omega_s = \sum_a \omega_a$ and $\chi^{(n)}$ is the nth order susceptibility. The numerical coefficients $C(-\omega_s;\omega_a,\ldots)$ arise from the Fourier expansion of the field and ensure that all susceptibilities of the same order have the same static limit. A tabulation can be found in Ref. [130]. Each of the susceptibilities corresponds to different physical processes: $\chi^{(1)}$ governs the refractive index, $\chi^{(2)}(-2\omega;\omega,\omega)$ the second harmonic generation (SHG), $\chi^{(3)}(-3\omega;\omega,\omega,\omega)$ the third harmonic generation (THG) and $\chi^{(3)}(-\omega;\omega,\omega,-\omega)$ the degenerate four-wave mixing (DFWN) or the intensity dependency of the refractive index.

The microscopic polarization of a molecule in an external field (or the dipole moment, i.e., the positions of the charges in the molecules averaged over the molecular volume) can be expanded in a Taylor series:

$$\begin{aligned} \mu_i^{\omega_s} = {} & \delta_{\omega_s,0}\mu_i^0 + \alpha_{ij}(-\omega_s;\omega_s)F_{\omega_s,j}^{tot} \\ & + \frac{1}{2}C(-\omega_s;\omega_a,\omega_b)\beta_{ijk}(-\omega_s;\omega_a,\omega_b)F_{\omega_a,j}^{tot}F_{\omega_b,k}^{tot} \\ & + \frac{1}{6}C(-\omega_s;\omega_a,\omega_c)\gamma_{ijkl}(-\omega_s;\omega_a,\omega_b,\omega_c)F_{\omega_b,j}^{tot}F_{\omega_b,k}^{tot}F_{\omega_c,l}^{tot} \end{aligned} \tag{3-82}$$

where the numerical coefficients C are the same as for the macroscopic polarization.

For extracting microscopic properties from experiment the so-called local field factors are needed [131], and, vice versa, also to obtain macroscopic values from computed (microscopic) results. The concept of relating the macroscopic field and the actual (or local) field experienced by a molecule goes back to Lorentz [113,132].

The idea is that only the field from molecules near to the solute has to be considered, so that the complete system can be separated into microscopic and macroscopic regions. The molecules in the latter can be described by the average macroscopic properties. Lorentz derived a simple relation between the local field and the macroscopic polarization, which is still in use [113,133,134,135].

DRF has been implemented such that all necessary information is available. To that end, we distinguish between 'solute' and 'effective' properties. The first coming from the action of a field solely on the solute in a cluster, but embedded in its classical environment. For the latter, the field acts on the whole discrete system, hence generating the field of dipoles induced by the field that counteract the inducing field.

From the effective properties the macroscopic polarization can be calculated as

$$P_I^{\omega_s} = N_\mathrm{d}\delta_{\omega_s,0}\left\langle \mu_i^{\mathrm{eff}} \right\rangle_I \tag{3-83}$$

with N_d the number density, and from there the local field factors, the refractive index and the susceptibilities. For details the reader is referred to Ref. [136].

3.3. SOME VALIDATION

Many applications of new force fields and new QM/MM methods of necessity focus on 'agreement' with experimental or otherwise calculated results. Also in this section we will first show that DRF indeed gives a reliable model for static and response potentials and can lead to QM/MM—or even completely MM calculations—that are as good as, e.g., SCF calculations. To that end we point at some results for simple systems like the water and benzene dimers, and the three- and four-body interactions in several systems.

3.3.1. The Water Dimer

The hydrogen-bonded water dimer is without any doubt the most used system to study intermolecular interactions, be it from the QM [34,72] QM/MM [13,26,31,32,40,52,108], or MM [25,42,45,48,50,72] perspective. In the past we have also used it to show that the DRF model indeed gives static and response potentials that are as good as, e.g., SCF calculations [74,137]. Of course, if this is the case, it allows for arbitrary separation of the total system into different subsystems, which can then be arbitrarily described at the QM or MM level; e.g., for a simple system like the water dimer, one may treat both monomers at the QM level, one monomer at QM and the other at MM, or both monomers at MM. Hence, we may go from the computationally expensive fully QM to QM/MM and to MM, without significant loss of accuracy. Alternatively, we can do MD simulations at the MM level, take snapshots from them and submit these to QM/MM (or QM) calculations to obtain UV-Vis spectra, excitation energies, NLO properties, etc., for the solute in solvent, i.e., *sequential* MD.

In order to show that this interchangeability is indeed feasible, we focus on the hydrogen-bonded water dimer (see Figure 3-2). We treated it first completely with

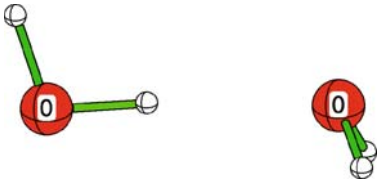

Figure 3-2. The hydrogen-bonded water dimer. The *x*-axis coincides with O–H–O

QM at the RHF level with Dunning's DZP basis set [138], and corrected for basis set superposition errors (BSSE) [102]. Next we treated it at the fully classical MM level, using the force field parameters as obtained from the RHF/DZP calculations on the monomer. Hence, we used atomic polarizability values (3.3791 a.u. for oxygen, 1.3333 a.u. for hydrogen) and an *a*-factor of 2.445 that result directly from polarizabilities calculated at the same level of theory (see, e.g., Table 4 in Ref. [60]). The partial charges on the atoms (–0.7886 on oxygen, 0.3943 on hydrogen) reproduce the dipole moment of the monomer at RHF/DZP calculation (2.28 D). Finally, the atomic radii (3.5587 a.u. for oxygen, 0.9637 a.u. for hydrogen), needed for the short-range repulsion (cf., Eq. 3-77), were taken from the atomic quadrupole moments (or rather, the expectation values of R^2) also from the RHF/DZP calculation.

With these force field parameters we calculated the potential energy surfaces for the water dimer (without taking dispersion into account since this is absent in RHF calculations) at the MM level using three different choices for the short-range repulsion. As already mentioned in the Section 3.2.5, the latter term is the only energy term that does not result directly from second-order perturbation theory. So far, we have been using the CHARMM expression Eq. (3-77) that takes the expression for the dispersion energy and 'corrects' it to give the Lennard-Jones repulsion term that goes as R^{-12}. In our early work, we took the CHARMM expression directly, i.e., without including the screening factors in the dispersion part that account for overlapping charge densities. More recently, we have moved on to including the screening factors to make it consistent with the other energy terms. Here, we explore for the first time also exponential repulsion, which should be more appropriate for the short-distance range.

In Figure 3-3 the excellent agreement between the fully QM and the fully MM data is seen, having minima at the same O–O distance with the same well depth. As anticipated, screening the repulsion for overlapping charge densities improves the agreement with the reference RHF/DZP data to some extent, but not much. The use of exponential repulsion does not play a major role here, but this may be resulting from using RHF as a method for obtaining the force field parameters.

In Figure 3-4 the experimental radial distribution [139] of water is plotted together with the one obtained with a 257 molecules MD simulation (with the same parameters as above) in which the central water molecule is the solute. The comparison is not bad: the first maxima for MM and experiment are almost at the same position. The second maximum (MM) is too far out, and the third maximum is virtually not

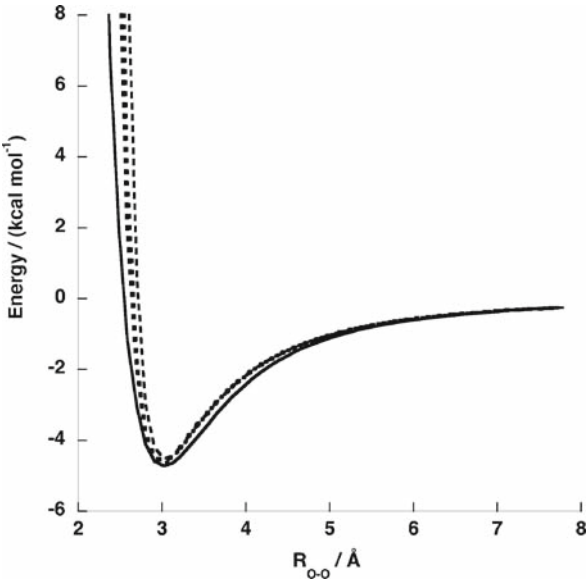

Figure 3-3. Potential energy surface for the water dimer obtained at RHF/DZP and fully classical MM levels with various repulsion models. *Solid line*: RHF. Repulsion; *dashed line*: unscreened LJ; *dotted*: screened LJ ; *bold dotted*: unscreened X6

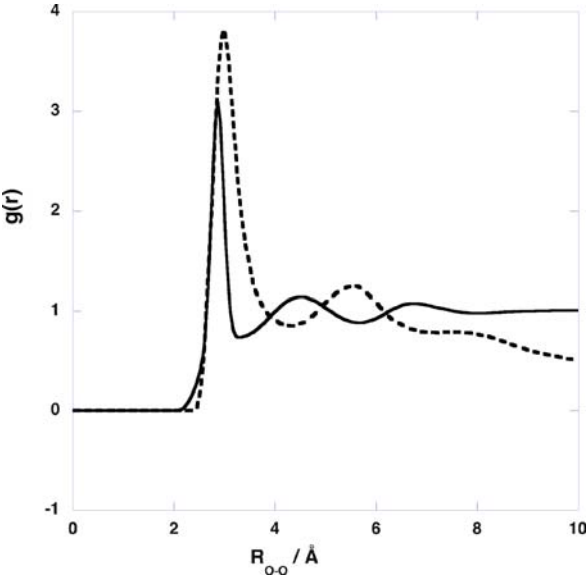

Figure 3-4. Radial distribution of 126 water molecules around the central water molecule from a MD simulation at 298 K with parameters from RHF/DZP calculation (*dashed line*) and experimental $g(r)$ (*solid line*) from Ref. [139]

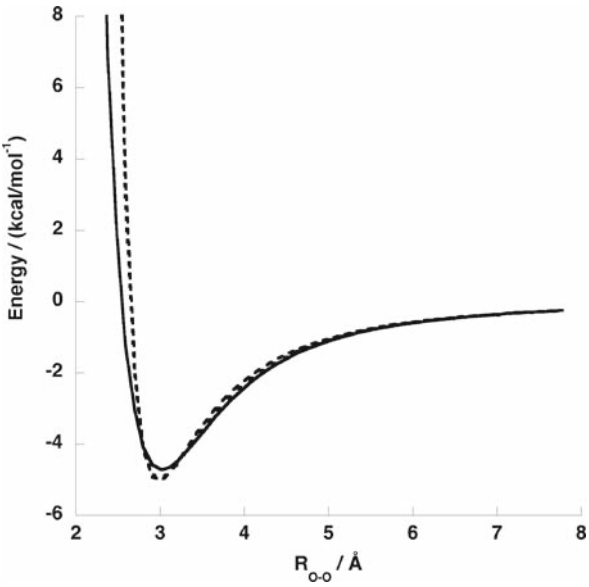

Figure 3-5. Potential energy surface for the water dimer obtained at RHF/DZP and QM/MM levels. *Solid line*: RHF; *dotted*: donor QM; *dashed*: acceptor QM

present. All these differences have to do with the parameterization based on the RHF results, and the size of the sample.

With this good agreement between the fully QM and fully MM results in mind, we went a step further and performed QM/MM calculations for the water dimer. There are two ways for separating the water dimer, i.e., either with the hydrogen-bond donor or the H-bond acceptor in the QM part. We calculated the PES for either QM/MM option, using the same force field parameters as before, and the 'exact' version of HONDO/DRF, i.e., (reaction) potentials and fields, were obtained as expectation values of the appropriated operators. In Figure 3-5 the QM/MM potential energy curves are plotted, together with the fully QM one.

The excellent agreement between the MM, QM/MM and QM PES results directly from the consistent and consequent screening of the interactions for overlapping charge densities. Therefore, as was already shown previously [74,137], our model gives static and response potentials that are as good as SCF calculations (and better if the dispersion is accounted for) which let us separate the total system into different subsystems.

3.3.2. Benzene Dimer

While the water dimer serves as the prototype system for studying hydrogen-bonding interactions, the benzene dimer serves this same purpose for π–π stacking. The latter may also be relevant for technological applications, but it is mainly associated with

biological systems such as deoxyribonucleic acid (DNA) or proteins. The benzene dimer proved to be a challenge for quantum-chemical methodologies. On the one hand, the system was too large for treatment with highly sophisticated ab initio methods such as CCSD(T) with large basis sets (which are necessarily large because the BSE is of the same order of magnitude or larger than the interaction itself), while more efficient QM methods (RHF, DFT) had intrinsic problems in describing accurately the dispersion interaction which is the major component of the interaction energy [140]. More recently, with improvements in computational power and DFT functionals, it has become possible to study these complexes more accurately [141,142].

Many different structures can be envisaged for the benzene dimer, but three stand out: parallel (P), parallel-displaced (PD) and T-shaped perpendicular (T) while for PD and T there are various orientations possible (See Figure 3-6).

We have studied the benzene dimer several times previously [74,87]. In the first one [74] only two structures (P1 and T2) were investigated, for which the geometry was taken directly from another study, with force field parameters obtained from a RHF/DZP calculation on the monomer. In the second, we studied five structures from Figure 3-6 [143], taking force field parameters from a DFT (BP86/TZ2P) calculation of the monomer, and performed a PES-scan for each of them. The dimer was investigated at the MM level in both studies, using different choices for the atomic charges and atomic polarizabilities.

The first non-vanishing multipole moment of the benzene molecule is the quadrupole moment, so the charges used within the MM calculations should give a good representation of it. The dipole-preserving charges (DPC) resulting from RHF/DZP, as used in the first study, give a molecular quadrupole moment of –2.82 a.u. (reported here is Θ_{zz}; because of symmetry $\Theta_{xx} = \Theta_{yy} = -1/2\ \Theta_{zz}$). This is a significant underestimation of the expectation value of the quadrupole at the same level, which amounts to –7.10 a.u. On the other hand, the multipole-derived (MDC-q) charges used in the second study represent by construction the computed molecular quadrupole moment (–5.59 a.u.), which is only slightly lower than the experimental value of –6.46 a.u. [143].

Because dispersion is an important component of the intermolecular interaction—in fact the most important for the relative stability of benzene dimers [140]—the value of the (molecular) polarizability is most likely very important for the stability

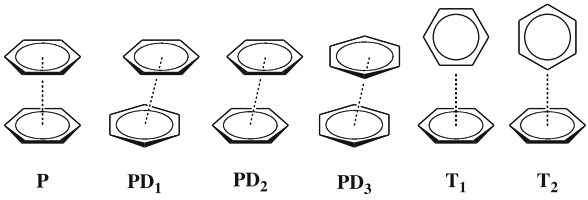

Figure 3-6. Structures of the various benzene dimers. For symbols used, see text

Table 3-5. Interaction of the benzene dimers (kcal/mol)

method	monomer properties		energies					
	α	θ	P	P1	P2	P3	T1	T2
DPC-[a]	61.5	–4.66	–	−2.20	–	–	–	–1.92
EE	70.1	–6.64	–	−3.18	–	–	–	–3.38
SMDC_vDS	70.1	–5.59	−1.63	−2.49	–2.56	–	–2.28	–2.26
CCSD(T)	–	–	−1.70	–	–	–2.63	–	–2.61
exp	70.1	–6.64			1.67±0.24[a,b]			

[a]Ref. [144]; [b]+ZPE: 1.87 kcal/mol.

of the isomers. The benzene molecule is a special molecule (like any other arene) in that the nuclear framework is planar, but an important portion of the electron density resides outside this plane. One-electron basis sets tied to the nuclei provide insufficient opportunity to distribute electrons in the regions above and below the molecular plane. The same holds for Thole's model, in which polarizabilities too are centered on atoms. This deficiency may lead to the underestimation of the out-of-plane component of the molecular polarizability tensor. The importance for the benzene dimer, and the relative stability of the different structures is, a priori, unclear. Therefore, in the first study, a set of polarizabilities outside of the nuclear plane was used, together with point charges fitted to give the experimental values. In Table 3-5 the results for the various choices are summarized.

The computed interaction energies for the different structures of the benzene dimer varies from ca. –1.6 to –3.4 kcal/mol, depending on the particular form and model used. From Table 3-5 we learn also that 'simply' choosing parameters that match experimental values (EE) does not work: these values are beyond any other results. Better are those of good QM calculations generating values for polarizabilities and charges being close to experiment, i.e., with the charges of Ref. [69] and the polarizabilities of Ref. [60] (SMC-vdDS) being in the range of high-quality ab initio calculations. Surprisingly, the most simple approximation (DPC) is closest to experiment: a dissociation energy of 1.92 kcal/mol at 5.03 Å, to be compared with 1.67 kcal/mol [140]—or rather 1.87 kcal/mol after correcting it for the zero point energy (ZPE) of 0.2 kcal/mol—for a T-shaped dimer at a distance of 4.96 Å [144]. The ZPE was obtained by fitting the CCSD(T) curve for the T-shaped dimer in Figure 4 of Ref. [141] to a Morse potential. The DPC result may be a fluke, but if so, and if we have to put more confidence in the numbers coming from, e.g., the CCSD(T) calculations, that would not be the first time that good ab initio calculations suggesta re-interpretation of the experimental findings [145]. More support for the DPC parameterization is collected in Table 3-6, where the results of MC-PESs are compared with experimental dissociation energies [140] of various benzene derivatives. Even if the numbers in Table 3-6 are corrected with ca. 0.2 for the ZPE, they are reasonably good.

Table 3-6. Interaction energies of benzene and derivative dimers (kcal/mol)

System	Structure	U_{MC}[a]	Experiment[b]
B–B	T2	−1.92	−1.67±0.24
B–T	P1	−3.35	−3.11±0.48
T–T	P1	−3.58	−3.35±0.48
T–X	P1	−4.18	−4.06±0.72
X–X	P1	−4.86	−5.02±0.72
F–F	P1	−3.66	

[a]Minimum of MC from Ref. [74] PES; [b]from Ref. [140].

3.3.3. Many-Body Interactions

Reacting on a remark of Chalasinski and Szczesniak [146] that classical polarization is a 'too poor model' to describe many-body effects, Grozema et al. [71] performed SCF and classical DRF calculations which showed that this insufficiency has probably more to do with particular polarization models than with classical models in general. The following partitioning of the total interaction energy was used:

$$\Delta U_{tot} = U^{(abc)} - U^{(abc)}(a) - U^{(abc)}(b) - U^{(abc)}(c) \tag{3-84}$$

with $U^{(abc)}(a)$ the energy of component a in the trimer (abc) basis set. All interactions were corrected for the BSSE applying the Boys–Bernardi counterpoise scheme [101,102]. The correlation-consistent basis set of Dunning [147] was used. For the classical calculations point charges giving the monomer dipoles and polarizabilities obtained from monomers with the same basis sets were used. For details, see Ref. [71]. Here some results are summarized in Table 3-7.

Extending this to a HF tetramer, the three- and four-body interactions were calculated, respectively, as –2.109 and –0.090 kcal/mol with SCF, and 2.055 and 0.126 kcal/mol with DRF. The relative success of the DRF model is most likely due to the fact that we always use self-consistent solutions of the expression in Eq. (3-47).

Table 3-7. Three-body interactions in some trimers (kcal/mol)

Method	HF	H_2O	Urea
SCF	−0.951	−0.987	−0.467
DRF	−0.920	−1.131	−0.498
Diff.	3%	15%	7%

3.3.4. Concluding the Validation

In the foregoing sections we have shown that the parameterization of DRF, based on good quality QM calculations (large basis set, correlated wave functions, multipole derived charges and polarizabilities fitted to experiment) on monomers, gives for two difficult and extreme examples, i.e., the water and benzene dimers, results good enough to define it as 'default' for QM/MM and MM calculations.

3.4. APPLICATIONS

In this section we present summaries of the DRF approach in various fields of computational chemistry, ranging from spectra and (hyper-)polarizabilities to chemical reactions in solution.

3.4.1. Sudden Polarization in Excited States of Symmetric Ethylenes

An interesting phenomenon is the so-called 'sudden polarization' in low-lying excited states of symmetric alkenes like (substituted) ethylenes. One aspect of the behavior of the excited states of these systems is the existence of a polarized (or charge separated) state in which two electrons are localized at one side of the molecules—as opposed to the initial 'biradical' state in which the unpaired electrons are distributed—and thus leading to a considerable dipole moment. Direct and indirect experimental evidence of such a 'phantom' state comes from time-resolved photo-induced excitation experiments on tetraphenylethylene (TPE) [148]. Other studies on TPE have revealed a strong correlation between the lifetime of this polarized excited state and solvent polarity. Schilling and Hilinsky [149] observed a dramatic drop in TPE excited state lifetime from several nanoseconds in non-polar solvents to only a few hundreds of picoseconds in (di)polar solvents. Picosecond optical calorimetric studies by Ma and Zimmt [150] showed a decrease of the energy gap between the ground and excited states of several (para-substituted) TPEs with increasing solvent polarity, which has led to the suggestion that the energy difference between ground and excited states is a measure of the coupling between the two states, thus explaining the decrease in lifetime of CT states in polar solvents.

After the vertical excitation of an electron from the D_{2h} ground state of ethylene, the C–C bond length will increase and a twist around this bond will be initiated. On progressing twisting, three low-lying excited singlet states arise, which at the perpendicular D_{2d} geometry are denoted as $N(^1B_1;ab)$, $V(^1B_2;a^2–b^2)$ and $Z(^1A_1;a^2+b^2)$ and are very sensitive to the twist angle. The N state is destabilized in going from the D_{2h} to the D_{2d} geometry, while in this process the V and Z states are stabilized, coming close together and—in the Born–Oppenheimer approximation—cross for $\theta \approx 80^\circ$. Around the near perpendicular geometry the V and Z are (nearly) degenerate and linear combinations of V and Z like $V \pm Z$ are equally acceptable solutions of the Schrödinger equation leading to localized states of type a^2 or b^2 which have a considerable dipole moment.

As a first effort to investigate the influence of solvents on the properties of these states, we prepared non-symmetrical reaction potentials in a continuum with various dielectric constants generated by putting a localized charge distribution for $\theta \approx 90^\circ$, obtained from a RHF procedure from which an a^2 solution was obtained with a dipole moment of about 4.0 D. This was done for dielectric constants ε = 2.0, 4.0, 6.0 and 10.0, which are typical for a range of organic solvents with increasing polarity. Configuration interaction with single and double excitations (CISD) in vacuo calculations on all valence electrons with the ROHF wave function as reference lead to perfectly zero dipoles for all states. With the polarized continuum present and starting from the localized RHF wave function at the D_{2d} geometry, a dipole moment of about 3.2 D was obtained, the strong polarization occurring near the crossing between the 'pure' V and Z states. It was found that a weak dielectric is unable to maintain a large dipole on progressive twisting beyond the $\theta \approx 80^\circ$ point, and we concluded that relatively strongly polar solvents are needed to trap polarized states in the near perpendicular geometry. Next we used DRF with ethylene in six different solvents [151]. First we calculated the polarizability of ethylene in its first excited state in the 70–90° twist angle area with the finite field method. From this we learned that an electric field of about 5×10^{-5} a.u. is sufficient for a full charge separation. The polarizability increases almost stepwise from 'normal' to about the unphysical value of 80,000 a.u. around the 81° twist. For other twist angles the dipole moment was linear in the applied field. Solvation effects were investigated by SMC calculations on ethylene embedded in 50 solvent molecules, followed by QM/MM, as before, with CISD. In Table 3-8 the average solvent-induced dipole moments are listed.

Table 3-8 shows that, as expected, only polar solvents are capable of breaking the symmetry of the ethylene excited states. This led to new experimental work on TPE in which the dynamics of the charge separation was studied [152]. A similar theoretical study on the solvent effect on the formation of charge transfer states in 9,9'-bianthryl [153] led to similar results and conclusions.

Table 3-8. Average solvent-induced dipole moments in the N, Z and V states for 81° twist angle

Solvent	$\lvert\mu_z\rvert$/ D		
	N-state	Z-state	V-state
Ethane	0.0	0.09	0.08
Tetrachloromethane	0.01	0.72	0.70
Chloroform	0.05	2.07	1.93
Carbon dioxide	0.09	2.62	2.37
Acetone	0.10	2.61	2.38

3.4.2. Spectra

Spectra are in most cases calculated as help by the interpretation of experiments, like by assigning (orbital) transitions. On the other hand, computed spectra are obviously an excellent way to validate QM and QM/MM procedures. Calculated vertical transitions may be convoluted to bands, thus mimicking the internal movements in a molecule. Sometimes solvent effects are accounted for by adding a single or a few solvent molecules, thus missing any 'bulk' effects. Also in this field the continuum approach is popular, then, however, only a single set of vertical transitions is obtained, which may be broadened, now to mimic also the band structure usually obtained for spectra in the condensed phases. Applying the SMC or SMD and QM/MM techniques one may average the excitations and oscillator strengths and use standard deviations in either to indicate the margins.

In several cases DRF has been successfully applied for calculating spectra of molecules in solution. Of late, we add the oscillator strengths of all transitions in equal-width energy intervals, the width depending on the required resolution, and—if different conformers of the solute are present—scaled with appropriate Boltzmann factors. The individual transitions may be convoluted for the vibrations. In this way the bands appear 'naturally' and this is about the closest one can come to simulate a real spectrometer. Here we summarize some results.

3.4.2.1. The n→ π transition in acetone*

Our first effort to compute a spectrum was on the solvent shift of the $n \rightarrow \pi^*$ transition in acetone [154] in various solvents by calculating the ground state and first excited state as restricted and open shell Hartree–Fock (RHF and ROHF) single determinant wave functions. The solvent was for comparison modeled by both the dielectric continuum and by discrete solvent molecules in which the solute/solvent configurations were obtained from Monte Carlo (MC) simulations. This was done the 'hard way' by using the DRF-QM/MM ground state energy in the MC procedure, i.e., for each accepted step also a ROHF calculation was done on the excited state. Due to the extremely high CPU demands of this procedure only a limited number of solvents (water, acetonitrile (MeCN) and tetrachloromethane (CCl_4)), solvent molecules (ca. 30) and MC steps (ca. 7000) were possible with a minimum basis (STO-3 G) [138] for the solute. In Table 3-9 some of the results are collected.

From Table 3-9 one learns that the continuum-only results are only for water in reasonable agreement with experiment. In contrast, the discrete solvent model leads, even in this very limited version, to shifts that compare well with experiment. Notice also that going from water to MeCN and CCl_4, the dispersion is of increasing importance: MeCN has an appreciable dipole moment but is also more polarizable than water, especially along the CN triple bond, while for CCl_4 the polarizability is the only parameter of importance.

In the next effort [187] to compute the same $n \rightarrow \pi^*$ excitation in acetone we applied the SMC technique: completely classical MC calculations produced 100 solvent-solute configurations that were afterwards subjected to DRF-QM/MM

Table 3-9. Computed excitation shifts (cm^{-1}) of acetone[a] relative to the gas-phase result in water, MeCN and CCl_4

Solvent model	Shift in H_2O[b]	Shift in MeCN[b]	Shift in CCl_4[b]
Continuum[c]	−1803 (+1624)	–1848 (+1579)	−2403 (+675)
Discrete[d]	+1639 (+2788)	+620 (+1597)	−216 (+411)
Discrete, MC average	+1821 ± 330	+ 922 ±310	−381 ±75
Experimental[e]	+1700 ± 200	+ 400 ±200	−350 ±200

[a]Vacuum excitation energy 26,962 cm^{-1} (exp. 36, 100 ±100 cm^{-1}, [180]).
[b]A negative value indicates a red shift. The values in parentheses are without dispersion.
[c]Boundary at 1.2 times the van der Waals radii.
[d]At lowest energy solute–solvent configuration from an all-classical MC run.
[e]From [181,180,182].

calculations. The advantages are clear: more solvents (eight), more solvent layers (about two, i.e., 40–52 solvent molecules), more MC steps (50,000) and a better basis set (DZP instead of STO). The results are depicted in Figure 3-7.

Although the still relatively small basis and the use of HF wave functions result in absolute excitations far away from the experimental value, the solvent shifts are very well reproduced. The need for dispersion is probably disputable, because it might only be connected with the uncorrelated wave functions. Wave functions that

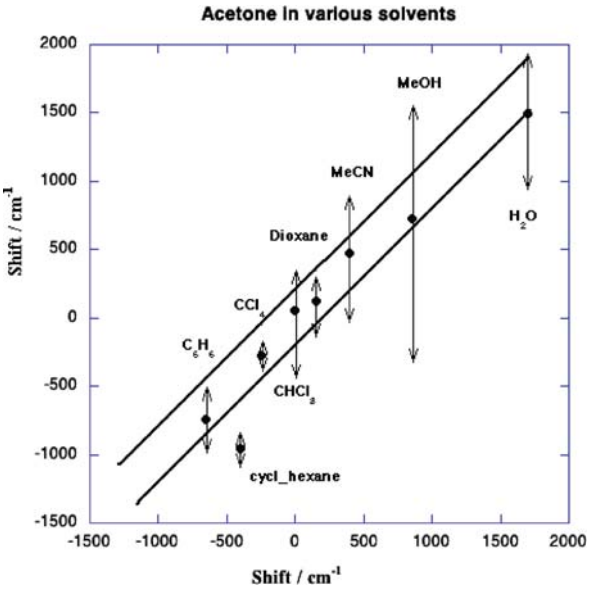

Figure 3-7. Calculated shifts of the $n \rightarrow \pi^*$ transition of acetone in various solvents. The *solid lines* indicate the experimental margins. The arrows indicate the standard deviations from the MC simulations. Data from Ref. [187]

do not violate the Pauli principle for the part in which there is overlap with charge distributions of solvent molecules, and in which electron correlation is accounted for, are more tight and lead possibly to less dispersion interaction. The most important issue here is the fact that all calculations were done with a single set of parameters, i.e., without reparameterization for, e.g., the excited state. The only difference was the adaptation of γ of Eq. (3-71), in which in the denominator the ionization energy of the solute was reduced by subtracting the calculated excitation energy, for use in the dispersion contribution of the excited state.

3.4.2.2. Absorption and emission spectra of N-(1-pyrenyl)-methyluracil-5-carboxamide-1-aminopyrene (PAU_{Me})

A more recent application is the calculation of the absorption and emission spectrum of a pyrenyldeoxyuridine nucleoside model [155] (see Figure 3-8). The interest was here to find an explanation for the stronger pyrenyl emission quenching in the polar solvents (MeCN and MeOH) than in the less polar solvent tetrahydrofuran (THF) [156]. This is consistent with the formation of intramolecular $Py^{\bullet+}/dU^{-}$ charge transfer (CT) states.

The absorption and emission spectra of *N*-acetyl-1-aminopyrene (PAAc) and PAU_{Me} immersed in 200 MeCN molecules were calculated using ZINDOs/CIS [84] and DRF [157] for the QM/MM parts. Eight conformers of both molecules were used, for PAAc obtained 'by hand' by rotating the Ac moiety, for PAU_{Me} as local minima in a classical MC calculation [156]. Each of the conformers was treated in a SMD simulation equilibrated to the vacuum ground state charge distribution as modeled by the ZDO [84] charges that reproduce the dipole moment, and a simulation equilibrated to the charge distribution of the first (vacuum) CT state. For each conformer 20 vertical transitions were calculated. The oscillator strengths were then scaled by appropriate Boltzmann factors, based on ground state energies calculated with the Amsterdam density functional package (ADF) [86], and then the ca. 15,000 transitions were collected in 200 equal-width energy intervals, leading to Figure 3-9 (PAAc) and Figure 3-10 (PAU_{Me}) in which we compare the calculated and experimental spectra. From Figure 3-9 we see that the combination ZINDO/DRF does reasonably well for PAAc, which made us going on with PAU_{Me}. Comparing the two spectra we see that the absorption bands for PAU_{Me} are much broader than for PAAc, which agrees with the experimental findings [156].

Both absorption and emission spectra are somewhat blue shifted, which we attributed to the difference between the spectroscopic model (PAUMe) and the compound actually used in the experiments (PAdU). Furthermore, the dispersion interaction was neglected, mainly because the choice of the scaling parameter γ Eq. (3-71) for states beyond the first excited state is cumbersome. Reducing the ionization energy of the solute by the excitation energy leads rapidly to a value smaller than zero, and hence to a positive dispersion interaction. In order to avoid this unphysical situation it is better to neglect the dispersion completely. Moreover, it is sometimes assumed that in semi-empirical wave functions electron correlation is accounted for because the parameters come from experiment. (The CIS

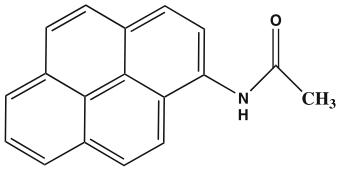

PAAc

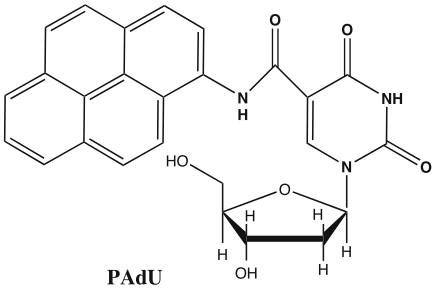

PAdU

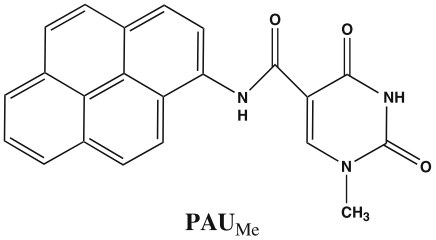

PAU$_{Me}$

Figure 3-8. Structural drawings of *N*-acetyl-1-aminopyrene (PAAc), 5-(*N*-carboxyl-1-aminopyrenyl)-2'-deoxyuridine (PAdU) and *N*-(1-pyrenyl)-1-methyluracyl-5-carboxamide (PAU$_{Me}$)

procedure of course, considering only single electron excitations, does not contribute to this). Reproduction of experimental spectra was not the main goal of this study, however satisfactory the results of Figure 3-10 may be. The events in the femtosecond experiments in Ref. [156] were rationalized as schematically pictured in Figure 3-11.

The left side of Figure 3-11 gives a qualitative impression of the computed spectrum for the solvent being equilibrated with the solute's ground state charge distribution. A relatively high-lying excited state is present with a very large dipole moment. The left side relates to a calculation for which the solvent is first equilibrated with the CT_1 state (in the gas phase). The effects are twofold: first the ground state shifts up,

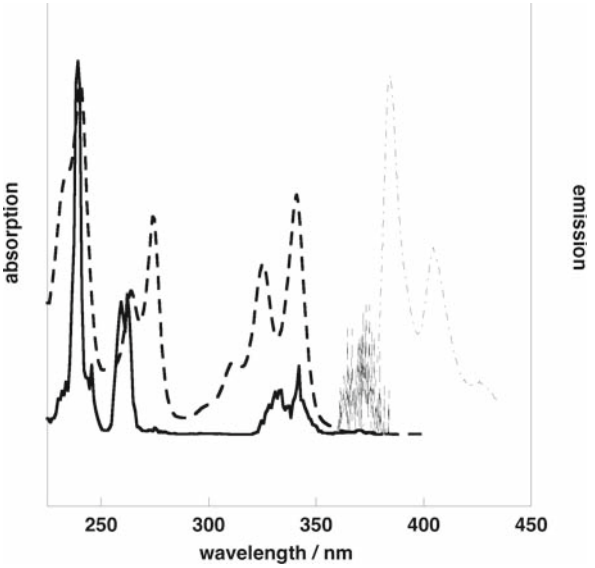

Figure 3-9. (Normalized) calculated (*solid*), experimental (*dashed*) absorption, and calculated (*dash-dot*) and experimental (*fine dash*) emission spectra of PAAc in MeCN

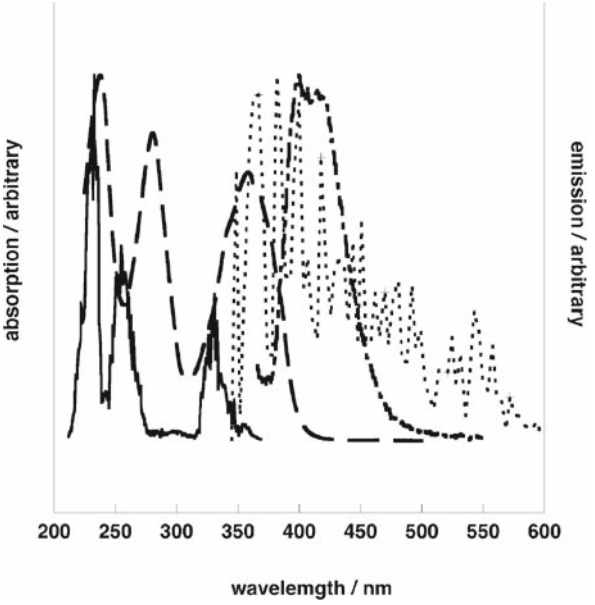

Figure 3-10. (Normalized) experimental (PAdU) and calculated (PAU_{Me}) absorption and emission spectra in MeCN. *Dashed line*: experimental absorption; *dash-dot*: experimental emission. *Solid line*: calculated absorption; *dotted line*: experimental emission

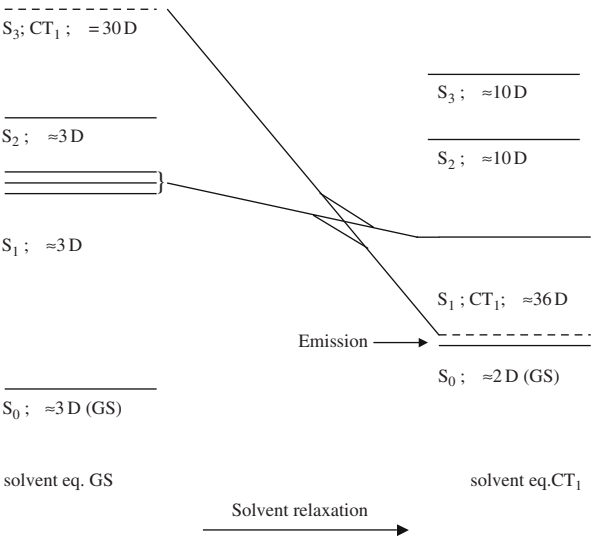

Figure 3-11. Schematic representation of two transition energy manifolds, showing some low-energy electronic states (S_n) of PAU_{Me} in MeCN. *Left*: solvent equilibrated with ground state charge distribution. *Right*: solvent equilibrated with charge distribution of (vacuum) CT_1 state

because it is not in equilibrium with the solvent. The other states may go up or down, depending on how much they 'like' their new environment. However, the CT_1 state is stabilized by almost 1 eV and actually ends up as the first excited state. This state lies very close to the (new) ground state, thus explaining the emission quenching of such states. For the details we refer the reader to Ref. [155].

3.4.2.3. The visible spectrum of Fe-(PyPepS)$_2^-$

Another numerical experiment involved a model active site of Fe-dependent nitrile-hydratase (Nhase), a non-heme Fe^{III} enzyme that catalyzes the hydration of nitriles to amides. The mechanism is as yet unknown and computational chemistry may be important to help unraveling it, provided the methods used are adequate, and the idea was that calculating the spectrum is a good check on the computational method. Of the model compound, $[Fe^{III}(PyPepS)_2]^-$ (see Figure 3-12) the spectrum in aqueous solution is known.

The spectrum is very similar to that of the native enzyme, showing strong absorption in the 400–500 nm region and a weaker band around 700–800 nm. An early effort to calculate it from a combination of time-dependent density theory TDDFT and MM (geometry optimization of the complex surrounded by 50 water molecules), followed by ZINDOs/CIS in which the whole sample was treated quantum-mechanically, failed for several reasons. Semi-empirical methods like INDO are minimal basis set approaches that are unable to describe negative ions. In the analysis of the charge distribution of the resulting SCF wave function all

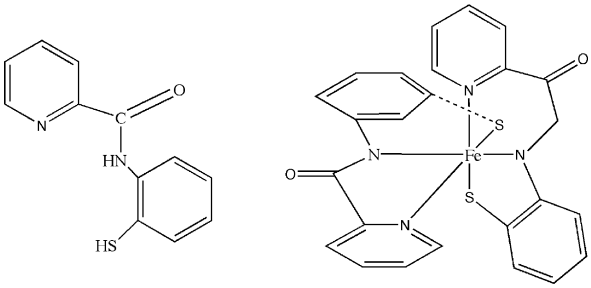

Figure 3-12. Structural drawings of $PyPepSH_2$ (*left*) and $[Fe^{III}(PyPepS)_2]^-$

water molecules were slightly negative to the extent that the complex 'lost' about two electrons and, hence, the calculated spectrum was that of a positive ion, rather than the original negative one. We turned to DRF that has been implemented in ZINDO for open shell ground states within the Rumer-CI scheme [158,159]. In the usual SMD/ZINDO/DRF procedure the spectrum was calculated for the complex immersed in 200 water molecules. The result was half satisfying: the 400–500 nm band was in perfect agreement with experiment but beyond 500 nm the spectrum was empty. This is probably due to the use of a minimal basis set for a negative ion, and the parameterization for Fe. Then we turned to TDDFT, using a DZ basis of Slater-type orbitals and arrived at the spectra in Figures 3-13 and 3-14 [160].

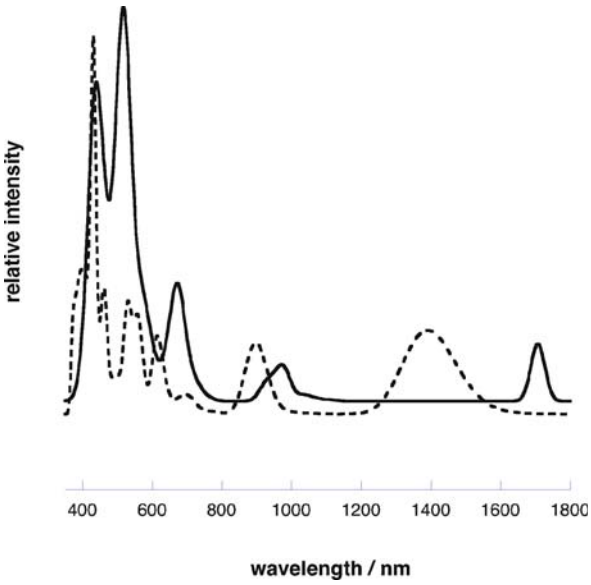

Figure 3-13. Gas phase spectrum (*solid line*) and spectrum of a single solute–solvent configuration (*dashed line*). Vertical transitions are convoluted by Gaussians with a width of 0.14 eV. Data from Ref. [160]

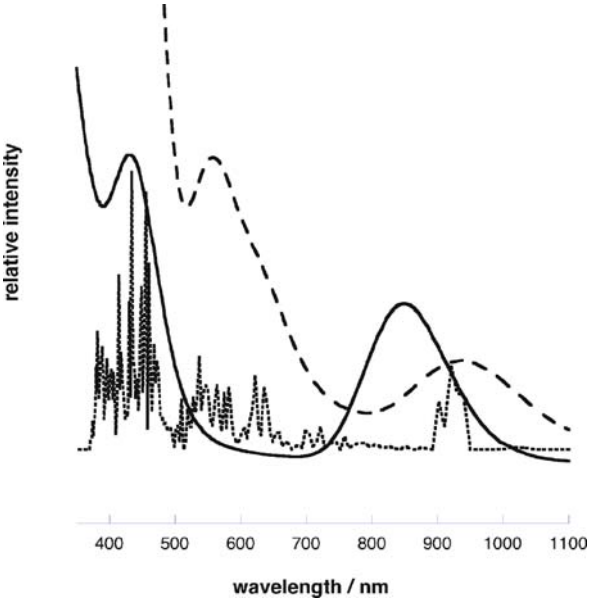

Figure 3-14. Experimental (*solid line*) and calculated (*dashed line*) spectra of $[Fe^{III}(PyPepS)_2]^-$ in water. Calculated spectrum obtained by collecting the vertical transitions of 25 solute–solvent configurations in 60 equal energy intervals, then convoluted with Gaussians with width of 0.3 eV. The dotted spectrum is collected in 200 intervals without convoluting

In Figure 3-13 the vacuum spectrum, comprising 100 vertical transitions, is superimposed on that of a single solute–solvent configuration. The latter shows the expected blue shift with respect to the gas phase: the excited state charge distribution sees a solvent polarization belonging to the ground state. In Figure 3-14 the spectrum is collected from 25 solute–solvent configurations and is compared with the experimental spectrum. It shows an overall red shift of about 70–120 nm. This means errors of ca. 0.3 eV in the high-energy part of the spectrum and ca. 0.1 eV in the low-energy region. This is more or less normal in spectra calculated with TDDFT [161,162,163]. The overall agreement with the experimental spectrum is satisfactory, and our conclusion is that this combination of TDDFT and DRF is promising for further investigations on the actual enzyme.

3.4.2.4. Circular dichroism spectrum of $[Co(en)_3]^{3+}$ in water

Chirality is an important topic in chemistry and biochemistry, due to the natural occurrence of chiral molecules in living organisms. In circular dichroism (CD) one measures the differential absorption of left- and right-handed circularly polarized light, which for chiral species are different. Therefore, CD has turned out to be a powerful tool which provides information on the electronic and geometric structure of chiral molecules. Since most CD spectra are measured in solution we extended our DRF/TDDFT method to also calculate such properties. As a first example we studied

the CD spectrum of a transition metal complex, $[Co(en)_3]^{3+}$, in aqueous solution [164]. Transition metal complexes are often chiral, so CD is used experimentally to characterize the compounds. The complex $[Co(en)_3]^{3+}$ represents a good benchmark system since there are several theoretical and experimental studies and since the CD spectrum of the complex is dominated by a single conformer.

The CD spectrum of the complex in aqueous solution was obtained by averaging over several snapshot configurations obtained from classical polarizable MD simulations. The convergence of the CD spectrum was shown to be quick with a required number of snapshots of the order of 50. It was demonstrated that by using mixed coarse/fine grained parallel computation this kind of averaging can be obtained within a few hours of turnaround time in a routine fashion.

Although, the DRF model predicts a blue shift of the CD bands above 35×10^3 cm^{-1}, a perfect agreement with experiment was not obtained since all the calculated intensities are much larger than what is found experimentally. Also, the DRF method predicts a weak band around 40×10^3 cm^{-1} which is not visible experimentally. The DRF results were compared with results obtained from the much simpler COSMO model, which showed very similar trends although larger shifts were found with the COSMO model. It was suggested that the weak band around 40×10^3 cm^{-1} was very sensitive to the local structure of the solvent, but this could be ruled out since the DRF results did not show a significant lowering of this band.

Although, the agreement with experiments did not show a significant improvement over the simpler COSMO model we are still confident that the combination of DRF with TDDFT is computationally an attractive solution for calculating chiro-optical properties of molecules in solution when the explicit solvent structure is of interest.

3.4.3. (Hyper-)polarizabilities and Macroscopic Properties in Solution

Non-linear optical (NLO) properties of molecules are very sensitive to solvent effects and it is therefore essential to include these effects directly in the calculations in order to accurately describe NLO properties. This makes the accurate prediction of molecular response properties in the condensed phase of great interest, both from a theoretical and a technological point of view, since materials exhibiting NLO effects are of fundamental technological importance for use in future application within electronics and photonics. Accurate calculations of NLO properties of molecules are difficult due to the strict requirements of the level of theory used, i.e., correlation and basis set with many diffuse functions are required. Attempts to calculate effective static (hyper)polarizabilities in the condensed phase go, in our group, 10 years back [110] in which we showed that it is to be expected that such properties are smaller than in the gas phase. The next one describes the static (hyper)polarizability of acetone in 11 different solvents, modeled with both the continuum and the discrete approach [24]. The conclusion was that in the continuum approach all values are larger, e.g., like in the work of Cammi et al. [165], Luo et al. [166] and Dehu et al. [167]. The latter two even suggest a strong correlation between the (non-)linear

Table 3-10. Comparison of the molecular properties of water in the gas phase. All results are in a.u.

Method	μ	α	β	γ
CCSD (gas)	0.73	9.52	−19.26	1942
DFT (gas)	0.71	9.97	−20.41	2021.3
Exp. (gas)	0.73	9.83	−19.2±5%	1800±8%
CCSD/MM	1.07	10.04	12.21	2169
DFT/DRF	1.04	10.13	8.57	2117.6

Data from Refs. [26,31,32].

properties and the dielectric constant of the solvent. This is a consequence of the inflation of density in a stabilizing-only environment, and the neglect of the role of the local fields. Wortmann and Bishop [131] pointed out that errors in the local field factors can lead to significant errors, both in calculated and experimental values. In contrast with the continuum approach, with discrete solvents [24,168] all effective static properties appeared to be smaller than in the gas phase for all solvents, and virtually independent of the dielectric constant. For example, α^{sol} is expected to be larger than α^{vac} for the reason given above: for a real solution the molecular charge distribution is stabilized. In contrast, $\alpha^{\text{eff}} < \alpha^{\text{vac}}$ due to the field from the dipoles induced in the immediate environment. At the time, in Ref. [24], a small basis set was used and all interaction (reaction) potentials and fields were expanded around the solute's nuclei [10]. With a single calculation using a large basis set and 'exact' potentials and fields, i.e., expectation values of the appropriate QM operators, the difference with the gas phase was much smaller.

Next, DRF was introduced in the response module of ADF [32] and the local field problem was reformulated and used to study solvent effects on the NLO properties of water, acetonitrile [26], *p*-nitroaniline (pNA) [169] and fullerene clusters. Here we summarize results for water and pNA since they are representative of the method.

3.4.3.1. Response properties of liquid water

Although water is not the first material that springs to mind when talking about NLO properties it has certain interesting properties. First, the size of the molecule is small, so that large basis sets and high-level theory can be used which provides a means of benchmarking new methods, a feature particularly important when dealing with TDDFT. In addition to this, water exhibits a sign change in the first hyperpolarizability upon solvation [170], a trend not reproduced with simple continuum models. As a benchmark of the DRF model we compared the results with coupled cluster (CCSD) results obtained both in the gas phase and for a single average water structure obtained from MD simulations [16]. The experimental and calculated results are summarized in Table 3-10.

From Table 3-10 it is clear that the DRF model compares extremely well with the results obtained from the more computational demanding CCSD method, both

in the gas phase and for the average liquid structure. The only exception seems to be the first hyperpolarizability where the DFT/DRF result is smaller than that of CCSD/MM. However, this difference probably arises from the short-range damping of the many-body polarization operator which is not included in the CCSD/MM model. The good agreement indicates that one needs only to benchmark the DFT in the gas phase. Although the small water cluster did not provide a realistic model of liquid water, it did provide a benchmark for the DRF model.

To go beyond a single average water structure, and capture the dynamic fluctuations of the properties of water molecules in liquid water, we selected 101 different water structures from a 50-ps SMD simulation of 256 water molecules. By comparing results from different configurations, information is obtained about the sensitivity of different response properties due to the dynamic fluctuations in the local molecular environment. This is illustrated in Figure 3-15 where the calculated linear polarizability, first hyperpolarizability and second hyperpolarizability are plotted as a function of the different configurations. All the properties show significant fluctuations, illustrating the importance of sampling over several molecular configurations in order to describe the solvent effect. This is particularly clear when considering the first hyperpolarizability that shows particularly large fluctuations. In fact, only on average does the first hyperpolarizability show the experimentally observed sign change [170], whereas many of the individual configurations retain a negative value.

While the above discussion clearly highlights the importance of including solvent effects in the calculations , the calculated properties cannot be compared directly with experimental results. This is mainly caused by the many different conventions used for representing hyperpolarizabilities and susceptibilities. However, the calculated properties can be combined with appropriate, calculated Lorentz/Onsager local field factors to obtain macroscopic susceptibilities that can be compared with experimental results. For water, we used this to calculate the refractive index and the third harmonic generation (THG) and the electric field-induced second harmonic (EFISH) non-linear susceptibilities. The results are collected in Table 3-11.

In order to make possible the comparison presented in Table 3-11 we converted the experimental values to match the conventions used in this work. Due to a myriad of different conventions used in defining the NLO properties this conversion is rather complicated but necessary when comparing with literature values. In addition to correcting for differences in conventions [129], we also adopted a different reference value for THG experiments on fused silica and EFISH experiments on quartz [171,172]. The combined effects of these, clearly makes a comparison between theory and experiments more difficult, since differences in convention and accuracy of reference values can obscure any agreement.

The agreement between the TDDFT/DRF results and experiment is very good for the refractive index and for the THG susceptibility. However, for EFISH we find that the theoretical results are smaller by almost a factor of three as compared with thewill be reflected in the snapshots and, therefore, hopefully describe the rotational contribution to the susceptibility.

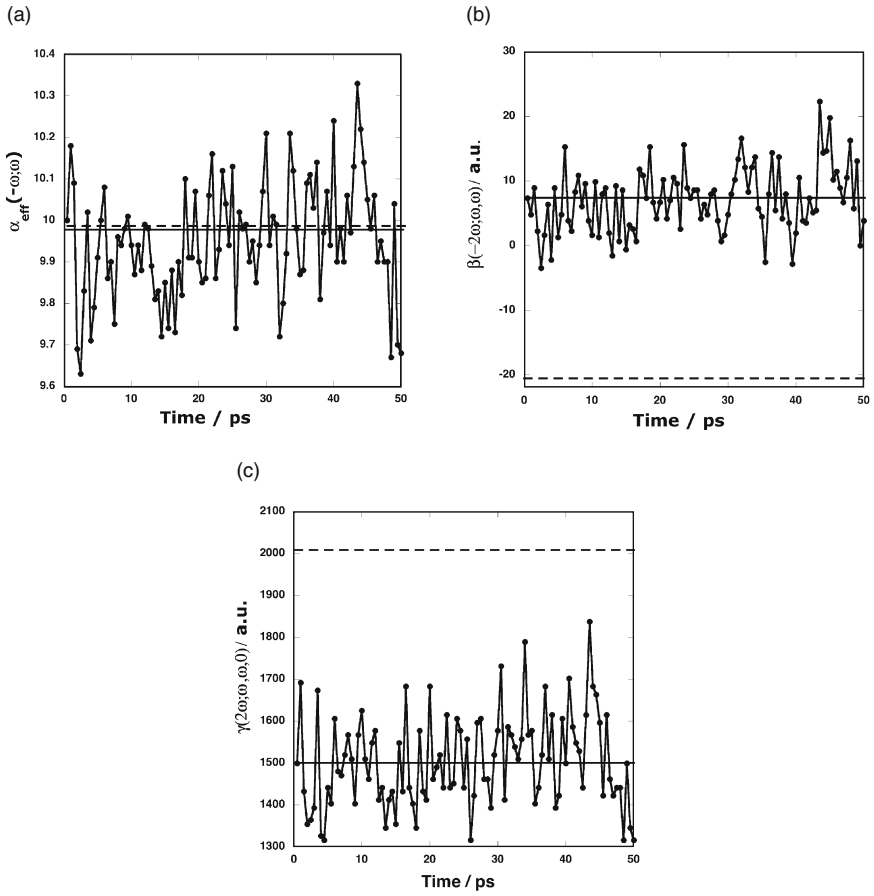

Figure 3-15. Fluctuations in effective linear polarizability (**a**), first (**b**) and second (**c**) hyperpolarizability as function of simulation time from 50 ps MD runs. Vacuum values (*dashed lines*) and average values (*solid lines*) are included

Table 3-11. Macroscopic response properties of liquid water. The frequency is $\omega = 0.0428$ a.u. $\chi^{(3)}$ is in units of 10^{-14} esu

	$n(\omega)$	$n(2\omega)$	$\chi^{(3)}_{\mathrm{THG}}$	$\chi^{(3)}_{\mathrm{EFISH}}$
DFT/DRF[a]	1.334	1.342	1.07	4.1
Exp.	1.326[b]	1.333[c]	1.29[b]	10.5[d]

[a]Ref. [26]; [b]Ref. [183]; [c]Ref. [184]; [d]Ref. [185].

3.4.3.2. The first hyperpolarizability of pNA in 1,4-dioxane solution

Molecules which contain donor and acceptor groups connected by some conjugated bridge (so-called push–pull molecules) are important candidates for new materials based on their strong NLO properties, particularly as SHG material. The prototypical push–pull molecule is *p*-nitroaniline (pNA) and it is therefore no surprise that there are numerous studies, both experimentally and theoretically, of its NLO properties. The molecular quantity that governs the SHG properties of materials is the first hyperpolarizability, $\beta(-2\omega; \omega, \omega)$, a quantity which can be measured using either with EFISH or hyper-Rayleigh scattering (HRS) techniques. In the gas phase the experimental value for the first hyperpolarizability of pNA is found to be 1072 ± 44 a.u. using the EFISH technique. In 1,4-dioxane solution values are found between 1359 and 1482 a.u. at 1064 nm using both HRS and EFISH measurements [129,171,173]. The increase in the first hyperpolarizability upon solvation in 1,4-dioxane is therefore found experimentally to be around 30%. We were therefore interested in seeing whether the DFT/DRF method can accurately describe the NLO properties of pNA and the increase due to solvation. Again, we performed SMD simulations of pNA in 1,4-dioxane solution, where 100 different solvent configurations, well separated in time, were selected. The results of the QM/MM calculations are presented in Table 3-12.

From Table 3-12 we see that the calculated solvent shift for β is calculated to be 30%, which is in excellent agreement with the experimental data. It is also evident that the calculated β is larger by a factor of two, both in the gas phase and in the solution. Several different possible causes of the differences between theory and experiments were explored. Calculations of β of a series of small molecules were all found to be in good agreement with experiments in the gas phase, indicating that the TDDFT method used can accurately describe the NLO properties [169]. To test the TDDFT/DRF model we also calculated the refractive index of 1,4-dioxane which shows good agreement with the experimental value. In the calculations we assumed that the structure of pNA is close to being planar which could explain some of the discrepancy between theory and experiment. Calculating β as an average over many pNA conformations is possibly the solution to this problem. On the other hand, this may also have to do with the problems TDDFT has with pull–push systems: in the

Table 3-12. Static and frequency-dependent properties of pNA in gas phase and 1,4-dioxane solution

Method	μ/D	β^{SHG}
DFT(gas)	7.73	2127
Exp(gas)	6.87	1072±44
DFT/DRF(1,4-dioxane)	10.62±0.06	2771±26
Exp. (1,4-dioxane)[a]	–	1359[a], 1409[a], 1482[b]

[a]Ref. [173]; [b]Ref. [186].

series of test calculations nitro-benzene also showed a β value from DFT that is more than twice the experimental one.

3.4.4. Chemistry in Solution

DRF is also used for modeling chemical events in solution. One example was used as a test to see if it could describe the simple dissociation of *ter*-butyl-chloride in water. The other is a numerical experiment on tautomerism of biologically important compounds, done because experiments are difficult or impossible.

3.4.4.1. The dissociation of ter*-butyl-chloride in water*

For describing the dissociation of *ter*-butyl-chloride (*t*ButCl), we performed MC calculations on $t\text{But}^+$, Cl^- and tetramethylammonium, $(CH3)_4N^+$ (TMA^+). TMA^+ is used as a benchmark because the experimental hydration energy of $t\text{But}^+$ is unknown. We calculated the 'solvated' minimal energy reaction path (MERP) as obtained from the gas phase, i.e., the Cl atom is stepwise removed from the central carbon atom, while the geometry of the *t*But group was optimized.

First Cl^-, $t\text{But}^+$ and TMA^+ were solvated by 62 water molecules, the temperature was 298 K, for equilibration 5×10^5 steps and for sampling 1×10^6 steps were used. This was repeated for the waters without solute, as reference. We used the Metropolis scheme without any sophistication. The charges on water were taken from ab initio calculations, the polarizabilities were set at the experimental values [60]. For the long-range interactions we added—for a number of accepted MC configurations—a dielectric continuum with $\varepsilon\approx80$. As boundary we took the solvent-accessible Connolly surface [174]. The free energy of cavitation was estimated from Pierotti's expression [175]. The results are given in Table 3-13.

The parameterization for Cl^- is apparently not perfect, most likely because the size is somewhat off. Noting that the experimental entropy change $\Delta S_{solv}(Cl^-)$ = –18.4 cal/(mol K) [176] the experimental change in enthalpy will—at 298 K—be $\Delta U_{solv}(Cl^-)$ = –81.4 kcal/mol, a number that must be compared with the –74 kcal/mol in Table 3-13.

The calculated free energy of TMA^+ is in good agreement with experiment, and therefore we had confidence in that for $t\text{But}^+$ as well. Next, we solvated 15 points along the vacuum MERP of the dissociation of *ter*-ButCl. We applied the MC

Table 3-13. Solvation energies (kcal/mol)

	ΔU_{int} [a]	ΔG_{solv} [a]	ΔG_{solv} [b]	ΔG_{tot}	ΔG_{exp}
$t\text{But}^+$	−43	−30	−15	−45	–
Cl^-	−74	–62	−19	−81	−76.0
TMA^+	−40	−34	−17	−51	−50.4

[a] From the MC calculations on the discrete system.
[b] Continuum contribution: $\Delta G_{solv} = \Delta G_{es} + \Delta G_{cav}$.

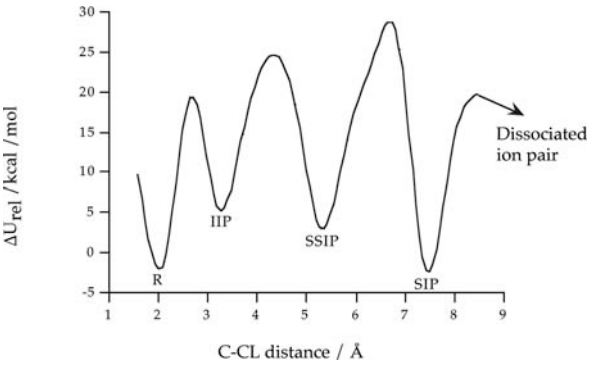

Figure 3-16. Minimum energy reaction path (MERP) for hydrolysis of *ter*-butyl-chloride (tBut) in water. Calculated was the potential of mean force for 15 points along the vacuum MERP of tBut immersed in 124 water molecules. For symbols see text

sampling again, now with 124 water molecules, adding the solvation energies to the corresponding values of the MERP energies, to arrive at the potential of mean force in solution by equilibrating each point on the MERP. Figure 3-16 gives an impression of the results.

From Figure 3-16, the four stages of Winstein [177] emerge clearly: the reactants (R), the intimate ion pair (IIP) at a longer C–Cl distance without water yet inserted, the solvent-separated IP with about a single water molecule between *t*But and the chloride ion, the solvent-separated IP (SSIP) and the separated IP(SIP) where both ions are solvated, but still strongly interacting, and, finally, the dissociated IP at infinite dilution. The calculated energy of activation (20 kcal/mol) for the rate-determining step, R→IIP, is in good agreement with the experimental value of Winstein et al. [176]. Even with this modest simulation the results are satisfactory, in particular because no specific parameterization was used. A similar study on the structure and stability of Li- and Na-carboxylate, -sulfate and -phosphate complexes is reported in Ref. [178].

3.4.4.2. Tautomerism of substituted cyclic imidazoline

The amidine group, –NH–C(R)=N– , occurs in numerous biologically active compounds, which include amino acids, antivirial, antibacterial, antifungal, antihypertensive drugs, and pesticides. Prototropic tautomerism in compounds containing this group is exceptionally difficult to study using the current experimental physicochemical methods because the proton transfer from the amino to the imino nitrogen is very fast and separation of individual tautomers is impossible. 2-Amino-2-imidazoline, 2-amino-2-oxazoline and 2-amino-2-thiazoline moieties are part of many important drugs (e.g., agonists and antagonists of α-adrenoreceptors, drugs binding to imidazoline receptors and inhibitors of neuronal Na^+ channels) and could be present in two tautomeric forms (amino and imino species). The absence of experimental energetic and structural data of amino–imino tautomeric equilibrium presents a

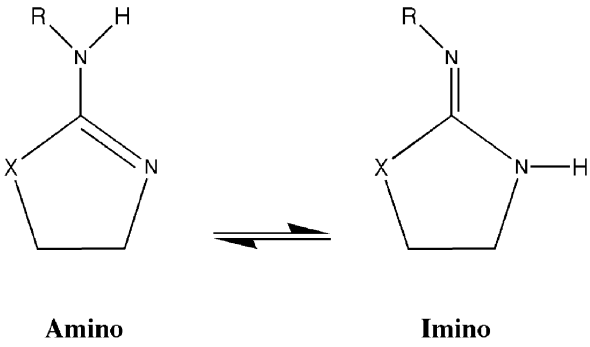

Figure 3-17. Scheme of amino–imino tautomerism, X=N, O; R=CH_3, Phenyl

challenge to quantum-chemical methods to obtain some insight into the reactivity of these compounds.

Here we summarize the results of a systematic theoretical examination of amino and imino tautomers in the systems schematically shown in Figure 3-17 based on DFT model chemistry in the gas phase and in water. In particular the equilibrium constant K_T = [amino tautomer]/[imino tautomer] for the process of Figure 3-17 was studied. The imino tautomers exhibit in general larger dipole moments and, hence are expected to have greater affinity to water and therefore a smaller K_T. In Table 3-14 the K_T values in the gas phase and in aqueous solution, obtained applying the MD module of DRF90 [87] for the solutes in 100 water molecules, are listed.

The values support the expectations on the shift of the equilibrium toward the imino form going from vacuum to solution with the exception of methyl derivatives of oxazoline and thiazoline of which the amino tautomers appear to be most

Table 3-14. Gas phase Gibbs energies and equilibrium constants[a]

	System	ΔG (kJ/mol)	K_T
1	Gas phase	−6	10
	Solution	30	6×10^{-6}
2	Gas phase	15	445
	Solution	3	4
3	Gas phase	−9	39
	Solution	−73	6×10^{12}
4	Gas phase	10	0
	Solution	70	6×10^{-13}
5	Gas phase	−9	44
	Solution	54	4×10^{-10}
6	Gas phase	8	23
	Solution	74	7×10^{-33}

[a]Data from Ref. [179].

stable in water. Probably the strong intramolecular hydrogen bonds of the N—H···O and N—H···S type, not present in the imino forms, play an important role. More information can be found in Ref. [179].

3.5. SUMMARY AND CONCLUSION

In this chapter we described the discrete reaction field (DRF) approach for handling condensed phase problems in computational chemistry. DRF focuses on a quantum-chemical treatment of the system of interest (the solute) while the rest of the (large) system is represented by discrete molecules or groups of atoms (the solvent) which are treated classically (QM/MM approach). The discrete parts are modeled by point charges and explicit polarizabilities obtained from high-level quantum-mechanical calculations on monomers without (or with minimal) fitting to experimental or to otherwise obtained results. This makes the parameters very transferable. Degrees of freedom of the solvent (MM) are treated by statistical mechanics techniques (e.g., molecular dynamics) with a force field that is parameterized in the same way. Although resulting in reasonable results, the least satisfying part of the force field used lies in the ad hoc short-range repulsion potentials needed to keep molecules sufficiently apart in (half) classical simulations. Because such potentials do not affect the electrons in QM/MM calculations, the electronic charge distributions are most likely too diffuse. This is a matter of further development.

We discussed DRF in perspective with other methods, gave the theoretical background and addressed the implementation. In a short section on the validation of DRF we showed that we can treat a system with QM, MM or QM/MM without significant loss of accuracy. A set of examples of its application ranges from simple solvation energies, spectra to (hyper)polarizabilities and processes of excited states of molecules in solution. These examples employ DRF in combination with—ab initio or semi-empirical—conventional wave function and DFT techniques.

We conclude that DRF is a flexible and reliable method for the treatment of condensed phase systems in computational chemistry.

ABBREVIATIONS

a.u.	atomic units energy: 1 a.u. = 1 Hartree = 627.5 kcal/mol = 2625.5 kJ/mol length: 1 a.u. = 1 Bohr = 52.917726 10^{-12} m charge: 1 a.u. = 1e = 1.60217733 10^{-19} C
ADF	Amsterdam density functional
AIMD	Ab initio molecular dynamics
ARF	Average reaction field
BSSE	Basis set superposition error
CT	Charge transfer
CCSD(T)	Coupled cluster with singles and doubles (+ perturbative triplets)
CD	Circular dichroism

CISD	Configuration interaction with singles and doubles
DFT	Density functional theory
DRF	Discrete (or direct) reaction field
DZP	Double-zeta + polarization functions
EFISH	Electric field induced second harmonic generation
ESP	Electrostatic potential
e.s.u	Electrostatic units
HF	Hartree-Fock
lhs	left hand side
MC	Monte Carlo
MCSCF	Multi-configurational self consistent field
MD	Molecular dynamics
MM	Molecular mechanics
MPn	Møller Plesset n-order perturbation
PCM	Polarizable continuum model
PES	Potential energy surface
PT	Perturbation theory
QM/MM	Quantum mechanics/molecular mechanics
RHF	Restricted Hartree-Fock
rhs	right hand side
ROHF	Restricted open shell Hartree-Fock
RP	Reaction potential
SAPT	Symmetry adapted perturbation theory
SCF	Self consistent field
SMC	Sequential Monte Carlo
SMD	Sequential molecular dynamics
TDDFT	Time dependent density functional theory
TZP	Triple zeta + polarization basis set

REFERENCES

1. Ballhausen, C., (1965) private communication.
2. Warshel, A. and Levitt M., *Theoretical studies of enzymatic reactions: dielectric, electrostatic, and steric stabilization of the carbenium ion in the reaction of Lysozyme.* J. Mol. Biol.: (1976) **103** 227–249.
3. Thole, B.T. and Duijnen P.Th. van, *On the quantum mechanical treatment of solvent effects.* Theor. Chim. Acta: (1980) **55** 307–318.
4. Singh, U.C. and Kollman P.A., *A combined ab initio quantum mechanical and molecular mechanical method for carrying out simulations on complex molecular systems: applications to the CH_3Cl + Cl^- exchange reaction and gas phase protonation of polyethers.* J. Comput. Chem.: (1986) **7** 718–730.
5. Bash, P.A., Field M.J. and Karplus M., *Free Energy Perturbation Method for Chemical Reactions in the Condensed Phase: A Dynamical Approach Based on a Combined Quantum and Molecular Mechanics Potential.* J. Am .Chem.Soc.: (1987) **109** 8092–8094.

6. Field, M.J., Bash P.A. and Karplus M., *A combined quantum mechanical and molecular mechanical potential for molecular dynamics simulations.* J. Comput. Chem.: (1990) **11** 700–733.
7. Karelson, M.M. and Zerner M.C., *Theoretical treatment of solvent effects on electronic spectroscopy.* J.Phys.Chem.: (1992) **96** 6949–6957.
8. Luzhkov, V. and Warshel A., *Microscopic models for quantum mechanical calculations of chemical processes in solutions: LD/AMPAC and SCAAS/AMPAC calculations of solvation energies.* J. Comput. Chem.: (1992) **13** 199–213.
9. Tomasi, J. and Persico M., *Molecular interactions in solution: an overview of methods based on continuous distributions of the solvent.* Chem. Rev.: (1994) **94** 2027–2094.
10. Vries, A.H. de, Duijnen P.Th. van, Juffer A.H., Rullmann J.A.C., Dijkman J.P., Merenga H. and Thole B.T., *Implementation of reaction field methods in quantum chemistry codes.* J. Comput. Chem.: (1995) **16** 37–55;1445–1446.
11. Jansen, G., Colonna F. and Ángyán J.G., *Mixed Quantum-Classical Calculations on the Water Molecule in Liquid Phase: Influence of a Polarizable Environment on Electronic Properties.* Int. J. Quantum Chem.: (1996) **58** 251.
12. Gao, J., *Hybrid Quantum and Molecular Mechanical Simulations: An Alternative Avenue to Solvent Effects in Organic Chemistry.* Accounts of Chemcal Research: (1996) **29** 298–305.
13. Tuñón, I., Martins-Costa M. T. C, Millot C., Ruiz-López M. F. and Rivail J. L., *A Coupled Density Functional-Molecular Mechanics Monte Carlo Simulation Method: The Water Molecule in Liquid Water.* J.Comput.Chem.: (1996) **17** 19–29.
14. Cramer, C.J. and Truhlar D.G., *Implicit Solvation Models: Equilibria, Structure, Spectra, and Dynamics.* Chem. Rev.: (1999) **99** 2161–2200.
15. Orozco, M. and Luque F.J., *Theoretical Methods for the Description of the Solvent Effect in Biomolecular Systems.* Chem. Rev.: (2000) **100** 4187–4225.
16. Poulsen, T.D., Ogilby P.R. and Mikkelsen K.V., *Linear repsonse for solvated molecules MC/SCF/MM.* J.Chem.Phys.: (2002) **116** 3730–3738.
17. Tomasi, J., *Thirty years of continuum solvation chemistry: a review, and prospects for the near future.* Theor.Chem.Acc: (2004) **112** 112–203.
18. Öhrn, A. and Karlström G., *A theoretical study of the solvent shift to the n-p transition in formaldehyde with an effective discrete quantum chemical solvent model including non-electrostatic perturbation.* Mol. Phys.: (2006) **104** 3087–3099.
19. Barone, V., Cossi M. and Tomasi J., *A new definition of cavities for the computation of solvation free energies by the polarizable continuum model.* J. Chem.Phys.: (1997) **107** 3210–3221.
20. Swart, M., Rösler E. and Bickelhaupt F.M., *Proton Affinities in Water of Maingroup-Element Hydrides. Effects of Hydration and Methyl Substitution.* Eur. J. Inorg. Chem.: (2007) 3646–3654.
21. Chen, F. and Chipman D.M., *Boundary element methods for dielectric cavity construction and integration.* J. Chem.Phys.: (2003) **119** 10289–10297.
22. Mennucci, B. and Tomasi J., *Continuum solvation models: A new approach to the problem of solute's charge distribution and cavity boundaries.* J. Chem.Phys.: (1997) **106** 5151–5158.
23. Cossi, M., Rega N., Scalmani G. and Barone V., *Polarizable dielectric model of solvation with inclusion of charge penetration effects.* J. Chem.Phys.: (2001) **114** 5691–5701.
24. Duijnen, P.Th. van, Vries A.H. de, Swart M. and Grozema F.C., *Polarizabilities in the Condensed Phase and the Local Fields Problem. A Direct Reaction Field formulation.* J.Chem.Phys.: (2002) **117** 8442–8453.
25. Rullmann, J.A.C. and Duijnen P.Th. van, *Analysis of discrete and continuum dielectric models; application to the calculation of protonation energies in solution.* Mol. Phys.: (1987) **61** 293–311.
26. Jensen, L., M.Swart and Duijnen P.Th. van, *Microscopic and macroscopic polarization within a combined quantum mechanics and molecuar mechanics model.* J. Chem.Phys.: (2005) **122** 034103.

27. Chalasinski, G. and Szczesniak M.M., *Origins of Structure and Energetics of van der Waals Clusters from ab Initio Calculations.* Chem. Rev.: (1994) **94** 1723–1765.
28. Wesolowski, T. and Warshell A., *Ab Initio Free Energy Perturbation Calculations of Solvation Free Energy Using the Frozen Density Functional Approach.* J.Phys.Chem: (1994) **98** 5183–5187.
29. Car, R. and Parinello M., *Unified approach for molecular dynamics and density-functional theory.* Phys.Rev.Lett.: (1985) **55** 2471–2474.
30. Gao, J. and Thompson M.A., eds. Combined Quantum Mechanical and Molecular Mechanics Methods. Vol. 712. 1998, ACS: Washington, DC.
31. Jensen, L., Duijnen P.Th. van and Snijders J.G., *A discrete solvent reaction field model for calculating molecular linear response properties in solution.* J.Chem.Phys.: (2003) **119** 12998–13006.
32. Jensen, L., Duijnen P.Th. van and Snijders J.G., *A discrete reaction field model within density functional theory.* J.Chem.Phys.: (2003) **118** 514–521.
33. Batista, E.R., Xantheas S.S. and Jónsson H., *Multipole moments of water molecules in clusters and ice Ih from first principles calculations.* J. Chem.Phys.: (1999) **111** 6011–6015.
34. DelleSite, L., Alevi A. and Lynden-Bell R.M., *The electrostatic properties of water molecules in condensed phases: an ab initio study.* Mol. Phys.: (1999) **96** 1683–1693.
35. Jensen, L., Astrand P.-O., Osted O., Kongsted J. and Mikkelsen K.V., *A dipole interaction model for the polarizability.* J. Chem. Phys.: (2002) **116** 4001–4010.
36. Engkvist, O., Åstrand P.-O. and Karlström G., *Accurate Intermolecular Potentials Obtained from Molecular Wave Functions: Bridging the Gap between Quantum Chemistry and Molecular Simulations.* Chem. Rev.: (2000) **100** 4087–4108.
37. Tu, Y. and Laaksonen A., *On the effect of Lennard-Jones parameters on the quantum mechanical and molecular mechanical coupling in a hybrid molecular dynamics simulation of liquid water.* J. Chem.Phys.: (1999) **111** 7519–7525.
38. Thole, B.T. and Duijnen P.Th. van, *The direct reaction field hamiltonian: analysis of the dispersion term and application to the water dimer.* Chem.Phys.: (1982) **71** 211–220.
39. Brooks, B.R., Bruccoleri R.E., Olafson B.D., States D.J., Swaminathan S.J. and Karplus M., *CHARMM: a program for macromolecular energy, minimization and dynamical calculations.* J. Comput. Chem.: (1983) **4** 187–217.
40. Rullmann, J.A.C. and Duijnen P.Th. van, *A polarizable water model for calculation of hydration energies.* Mol. Phys.: (1988) **63** 451–475.
41. Rullmann, J.A.C., Bellido M.N. and Duijnen P.Th. van, *The active site of Papain. All-atom study of interactions with protein matrix and solvent.* J. Mol. Biol.: (1989) **206** 101–118.
42. Ahlström, P., Wallqvist A., Engström S. and Jönsson B., *A molecular dynamics study of polarizable water.* Mol. Phys.: (1989) **68** 563–581.
43. Kuwajima, S. and Warshel A., *Incorporating Electric Polarizabilities in Water-Water Interaction Potentials.* J.Phys. Chem.: (1990) **94** 460–466.
44. Dang, L.X., *Development of nonadditive intermolecular potentials using molecular-dynamics - solvation of Li+ and F- ions in polarizable water.* J. Chem.Phys.: (1992) **96** 6970–6977.
45. Soetens, J.-C. and Milot C., *Effect of distributing multipoles and polarizabilities on molecular dynamics simulations of water.* Chem. Phys. Lett.: (1995) **235** 22–30.
46. Thomson, M.A. and Schenter G.K., *Excited States of the Bacteriochlorophyll b Dimer of Rhodopseudomonas viridis: A QM/MM Study of the Photosynthetic Reaction Center That Includes MM Polarization.* J. Phys. Chem.: (1995) **99** 6374–386.
47. Day, P.N., Jensen J.H., Gordon M.S., Webb S.P., Stevens W. J., Krauss M., Garmer D., Bash H. and Cohen D., *An effective fragment method for modeling solvent effects in quantum mechanical calculations.* J. Chem.Phys.: (1996) **105** 1968–1986.

48. Dang, L.X. and Chang T.-M., *Molecular dynamics study of water clusters, liquid, and liquid–vapor interface of water with many-body potentials.* J. Chem.Phys.: (1997) **106** 8149–8159.
49. Gao, J., *Energy components of aqueous solution: Insight from hybrid QM/MM simulations using a polarizable solvent model.* J. Comput. Chem.: (1997) **18** 1061–1071.
50. Burnham, C.J., Li J., Xantheas S. and Leslie M., *The parametrization of a Thole-type all-atom polarizable water model from first principles and its application to the study of water clusters (n=2–21) and the phonon spectrum of ice Ih.* J. Chem.Phys.: (1999) **110** 4566–4581.
51. Halgren, T.A. and Damm W., *Polarizable force fields.* Curr. Opin. Struct. Biol.: (2001) **11** 236–242.
52. Poulsen, T., Kongsted J., Osted A., Ogilby P.R. and Mikkelsen K.V., *The combined multiconfigurational self-consistent-field/molecular mechanics wave function approach.* J. Chem.Phys.: (2001) **115** 2393–2400.
53. Dupuis, M., Aida M., Kawahsima Y. and Hirao K., *A polarizable mixed Hamiltonian model of electronic structure for micro-solvated excited states. I. Energy and gradients formulation and application to formaldehyde..* J.Chem.Phys.: (2002) **117** 1242–1255.
54. Jorgensen, W.L., Chandraskhar J., Madura J.D., Impey R.W. and Klein M.L., *Comparison of simple potential functions for simulating liquid water.* J.Chem.Phys.: (1983) **79** 926–935.
55. Rullmann, J.A.C. and Duijnen P.Th. van, *Potential energy models of biological macromolecules: a case for ab initio quantum chemistry.* CRC Reports in Molecular Theory: (1990) **1** 1–21.
56. Kongsted, J., Osted A., Mikkelsen K.V. and Christiansen O., *Molecular electric properties of liquid water calculated using the combined coupled cluster/molecular mechanics method.* J. Mol.Struct. (THEOCHEM): (2003) **632** 207–225.
57. Applequist, J., Carl J.R. and Fung J.K., *Atom dipole interaction model for molecular polarizability. Application to polyatomic molecules and determination of atom polarizabilities.* J.Am.Chem.Soc.: (1972) **94** 2947–2952.
58. Silberstein, L., *Molecular refractivity and atomic interaction. II.* Philos.Mag: (1917) **33** 521–533.
59. Thole, B.T., *Molecular polarisabilities calculated with a modified dipole interaction.* Chem.Phys.: (1981) **59** 341–350.
60. Duijnen, P.Th. van and Swart M., *Molecular and atomic polarizabilities.* J.Phys.Chem.A.: (1998) **102** 2399–2407.
61. Mooij, W.T.M., Duijneveld F.B. van, Rijdt J.G.C.M. van Duijneveldt-van de and Eijck B.P. van, *Transferable ab Initio Intermolecular Potentials. 1. Derivation from Methanol Dimer and Trimer Calculations.* J. Phys. Chem. A: (1999) **103** 9872–9882.
62. Kaminski, G. A., Stern H. A., Berne B. J., Friesner R. A., Cao Y. X., Murphy R. B., Zhou R. and Halgren T. A., *Development of a Polarizable Force Field For Proteins via Ab Initio Quantum Chemistry: First Generation Model and Gas Phase Tests.* J.Comput.Chem.: (2002) **23** 1515–1531.
63. Ren, P. and Ponder J.W., *Consistent Treatment of Inter- and Intramolecular Polarization in Molecular Mechanics Calculations.* J. Comput. Chem.: (2002) **23** 1497–1506.
64. Kaminski, G. A., Friesner R. A. and Zhou R., *A Computationally Inexpensive Modification of the Point Dipole Electrostatic Polarization Model for Molecular Simulations.* J.Comput.Chem.: (2003) **24** 267–276.
65. Yu, H. and Gunsteren W.F. van, *Accounting for polarization in molecular simulation.* Comp. Phys. Comm.: (2005) **172** 69–85.
66. Elking, D., Darden T. and Woods R.J., *Gaussian Induced Dipole Polarization Model.* J. Comput. Chem.: (2006) **28** 1261–1274.
67. Møller, C. and Plesset M.S., *Note on an Approximation Treatment for Many-Electron Systems.* Phys.Rev.: (1934) **46** 618–622.

68. Breneman, C.M. and Wiberg K.B., *Determining atom-centered monopoles from molecular electrostatic potentials. The need for high sampling density in formamide conformational analysis.* J. Comput. Chem.: (1990) **11** 361–373.
69. Swart, M., Duijnen P.Th. van and Snijders J.G., *A charge analysis derived from an atomic multipole expansion.* J.Comput.Chem.: (2001) **22** 79–88.
70. Bachrach, S. M., ed. *Population Analysis and Electron Densities from Quantum Mechanics*. Reviews of Computational Chemistry, ed. K.B. Lipkowitz and D.B. Boyd. Vol. 5. 1994, VCH: Weinheim. 171–227.
71. Grozema, F., Zijlstra R.W.J. and Duijnen P.Th. van, *Many-body interactions calculated with the direct reaction field model.* Chem.Phys.: (1999) **246** 217–227.
72. Bukowski, R., Szalewicz K., Groenenboom G.C. and Avoird A.van der, *Predictions of the Properties of Water from First Principles.* Science: (2007) **315** 1249–1252.
73. Axilrod, P. M. and Teller E., *Interaction of the van der Waals Type Between Three Atoms.* J. Chem. Phys.: (1943) **11** 299–300.
74. Duijnen, P.Th. van and Vries A.H. de, *The "direct reaction field" force field: a consistent way to connect and combine quantum-chemical and classical descriptions of molecules.* Int. J. Quantum Chem.: (1996) **60** 1111–1132.
75. Broer, R., Duijnen P.Th. van and Nieuwpoort W.C., *Ab initio molecular orbital calculations on the active site of papain.* Chem. Phys. Lett.: (1976) **42** 525–529.
76. Thole, B.T., Duijnen P.Th. van and Hol W.G.J., *On the role of the active site a-helix in papain.* Biophys. Chem.: (1979) **9** 273–280.
77. Duijnen, P.Th. van, Thole B.T., Broer R. and Nieuwpoort W.C., *Active-site a-helix in papain and the stability of the ion-pair* $RS^{-}\ldots ImH^{+}$. Int. J. Quantum Chem.: (1980) **17** 651–671.
78. Thole, B.T. and Duijnen P.Th. van, *Reaction field effects on proton transfer in the active site of Actinidin.* Biophysical Chemistry: (1983) **18** 53–59.
79. Duijnen, P.Th. van and Thole B.T., *Environmental effects on proton transfer. Ab initio calculations on systems in a semi-classical, polarizable environment.*, in Quantum Theory of Chemical Reactions., R. Daudel, et al., Editors. 1982, D.Reidel Publishing Company: Dordrecht. p. 85–95.
80. Dijkman, J.P. and Duijnen P.Th. van, *Papain in aqueous solution and the role of Asp-158 in the mechanism: an ab initio SCF+DRF+BEM study.* International Journal of Quantum Chemistry, Quantum Biology Symposium: (1991) **18** 49–59.
81. Coutinho, K., Oliveira M.J.D. and Canuto S., *Sampling configurations in Monte Carlo simulations for quantum mechanical studies of solvent effects.* Int. J. Quantum Chem.: (1998) **66** 249–253.
82. Coutinho, K. and Canuto S., *The sequential Monte Carlo-quantum mechanics methodology. Application to the solvent effects in the Stokes shift of acetone in water.* J. Mol.Struct. (THEOCHEM): (2003) **632** 235–246.
83. Dupuis, M., Farazdel A., Karma S.P. and Maluendes S.A., *HONDO: a general atomic and molecular electronic structure system*, in MOTECC-90, E. Clementi, Editor. 1990, ESCOM: Leiden. p. 277–342.
84. Zerner, M.C., *ZINDO, A General Semi-empirical Program Package*. 1990, Quantum Theory Project, University of Florida: Gainesville (Fl.) USA.
85. Guest, M.F., Lenthe J.H. van, Kendrick J. and Sherwood P., *GAMESS(UK)*. 1999, Daresbury Laboratory: Cheshire England.
86. Baerends, E.J., Autschbach J., Bérces A., Bickelhaupt F.M., Bo C., Boerrigter P.M., Cavallo L., Chong D.P., L. Deng, Dickson R.M., Duijnen P.Th. van, Ellis D.E., Faassen M. van, L. Fan T.H. Fischer, Guerra C. Fonseca, Gisbergen S.J.A. van, Groeneveld J.A., Gritsenko O.V., Grüning M., Harris F.E., Hoek P. van den, Jacob C.R., Jacobsen H., Jensen L., Kessel G. van, Kootstra F., Lenthe E. van, McCormack D.A., Michalak A., Neugebauer J., Nicu V.P.,

Osinga V.P., Patchkovskii S., Philipsen P.H.T., Post D., Pye C.C., Ravenek W., Ros P., Schipper P.R.T., Schreckenbach G., Snijders J.G., Solà M., Swart M., Swerhone D., Velde G. te, Vernooijs P., Versluis L., Visscher L., Visser O., Wang F., Wesolowski T.A., Wezenbeek E.M. van, Wiesenekker G., Wolff S.K., Woo T.K., Yakovlev A.L. and Ziegler T., *Amsterdam Density Functional Theory*. 2007, SCM: Amsterdam.

87. Swart, M. and Duijnen P.Th. van, *DRF90: a Polarizable Force Field.* Mol. Simul.: (2006) **32** 471–484.
88. McWeeny, R., *Methods of Molecular Quantum Mechanics*. 1989, London: Academic Press.
89. Mehler, E.L., *Self-consistent, nonorthogonal group function approximation for polyatomic systems. I. Closed shells.* J.Chem.Phys.: (1977) **67** 2728–2739.
90. Mehler, E.L., *Self-consistent, nonorthogonal group function approximation for polyatomic systems. II. Analysis of noncovalent interactions.* J.Chem.Phys.: (1981) **74** 6298–6306.
91. Mehler, E.L., *Self-consistent, nonorthogonal group function approximation: An ab initio approach for modelling interacting fragments and environmental effects.* J. Mathematical Chemistry: (1992) **10** 57–91.
92. Stone, A. J., *The Theory of Intermolecular forces*. 1996, Oxford: Clarendon.
93. Kutzelnigg, W., *Stationary perturbation theory.* Theor. Chim. Acta: (1992) **83** 263–312.
94. Buckingham, A.D., *Basic theory of intermolecular forces: applications to small molecules*, in Intermolecular Interactions: From Diatomics to Biopolymers, B. Pullman, Editor. 1978, John Wiley & Sons: Chichester. p. 1–67.
95. Avoird, A. van der, Wormer P.E.S., Mulder F. and Berns R.M., *Ab initio studies of the interactions in van der Waals molecules*, in Topics in Current Chemistry, F.L. Boschke, Editor. 1980, Springer Verlag: Berlin. p. 1–51.
96. Margenau, M. and Kestner N. R., *Theory of Intermolecular forces*. 1969, Oxford: Pergamon.
97. Unsöld, A., *Quantentheorie des Wasserstoffmolekülions und der Born-Landéschen Abstoßungskräfte.* Z.Phys.: (1927) **43** 563–574.
98. London, F., *Theory and systematics of molecular forces.* Z.Phys.: (1930) **63** 245–279.
99. Casimir, H.B.G. and Polder D., *The Influence of Retardation on the London-van der Waals Forces.* Phys. Rev.: (1948) **73** 360–372.
100. Claverie, P., *Elaboration of approximate formulas for the interaction between large molecules: application in organic chemistry*, in Intermolecular Interactions: From Diatomics to Biopolymers, B. Pullman, Editor. 1978, John Wiley & Sons: Chichester. p. 69–305.
101. Boys, S.F. and Bernardi F., *The calculation of small molecular interactions by the differences of separate total energies. Some procedures with reduced errors.* Mol. Phys.: (1970) **19** 553–566.
102. Duijneveldt, F.B. van, Rijdt J.G.C.M. van Duijneveldt-van de and Lenthe J.H. van, *State of the art in counterpoise theory.* Chem. Rev.: (1994) **94** 1873–1885.
103. Thole, B.T. and Duijnen P.Th. van, *A general population analysis preserving the dipole moment.* Theor. Chim. Acta: (1983) **63** 209–221.
104. Mulliken, R.S., *Electronic population analysis on LCAO–MO molecular wave functions II. Overlap populations, bond orders, and covalent bond energies.* J.Chem.Phys.: (1955) **23** 1841–1846.
105. Jensen, F., *Introduction to Computational Chemistry*. 1999, Chichester, UK: Wiley.
106. Wiberg, K.B. and Rablen P.R., *Comparison of atomic charges derived via different procedures.* J.Comput.Chem.: (1993) **14** 1504–1518.
107. Sigfridsson, E. and Ryde U., *Comparison of methods for deriving atomic charges from the electrostatic potential and moments.* J.Comput.Chem.: (1998) **19** 377–395.
108. Jensen, L., Swart M., Duijnen P.Th. van and Snijders J.G., *Medium perturbations on the molecular polarizability calculated with a localized dipole interaction model.* J.Chem.Phys.: (2002) **117** 3316–3320.

109. Augspurger, J.D. and Dykstra C.E., *Evolution of polarizabilities and hyperpolarizabilities with molecular aggregation: A model study of acetylene clusters.* Int.J. Quantum Chem.: (1992) **43** 135–146.
110. Duijnen, P.Th. van, Swart M. and Grozema F., *QM/MM calculation of (hyper)polarizabilities with the DRF approach.*, in Hybrid Quantum Mechanical and Molecular Mechanics Methods, J.Gao and M.A. Thompson, Editors. 1999, ACS Books: Washington, DC. p. 220–232.
111. Kirtman, B., Dykstra C.E. and Champagne B., *Major intermolecular effects on nonlinear electrical response in a hexatriene model of solid state polyacetylene.* Chem.Phys.Lett.: (1999) **305** 132–138.
112. Fraga, S., Saxena K.M.S. and Karwowski J., *Handbook of Atomic Data*. Physical Sciences Data 5. 1976, Amsterdam: Elsevier.
113. Böttcher, C.J.F. and Bordewijk P., *Theory of electric polarization*. 2nd ed. Vol. II. 1978, Amsterdam: Elsevier.
114. Sadlej, A.J., *Medium-size polarized basis-sets for high-level-correlated calculations of molecular electric properties. 4. Third row atoms - Ge through Br.* Theor. Chim. Acta: (1991) **81** 45–63.
115. Sadlej, A.J., *Medium-size polarized basis-sets for high-level-correlated calculations of molecular electric properties. 5. Fourth row atoms - Sn through I.* Theor. Chim. Acta: (1991) **81** 339–354.
116. Werner, H-H. and W.Meyer, *Static dipole polarizabilities of small molecules.* Mol. Phys.: (1976) **31** 855–872.
117. Gisbergen, S.J.A. van, Osinga V.P., Gritsenko O.V., Leeuwen R. van, Snijders J.G. and Baerends E.J., *Improved density functional theory results for frequency-dependent polarizabilities, by the use of an exchange-correlation potential with correct asymptotic behavior.* J.Chem.Phys.: (1996) **105** 3142–3161.
118. Champagne, B., Perpète E.A., Gisbergen S.J. A. van, Baerends E.J., Snijders J.G., Soubra-Ghaoui C., Robins K.A. and Kirtman B., *Assessment of conventional density functional schemes for computing the polarizabilities and hyperpolarizabilities of conjugated oligomers: An ab initio investigation of polyacetylene chains.* J.Chem.Phys.: (1998) **109** 0489–10498.
119. Gisbergen, S.J.A. van, Schipper P.R.T., Gritsenko O.V., Baerends E.J., Snijders J.G., Champagne B. and Kirtman B., *Electric Field Dependence of the Exchange-Correlation Potential in Molecular Chains.* Phys. Rev. Lett.: (1999) **83** 694–697.
120. Gritsenko, O. and Baerends E.Jan., *Asymptotic correction of the exchange – correlation kernel of time-dependent density functional theory for long-range charge-transfer excitations.* J.Chem.Phys.: (2004) **121** 655–660.
121. Neugebauer, J., Gritsenko O. and Baerends E.J., *Assessment of a simple correction for the long-range charge-transfer problem in time-dependent density-functional theory.* J.Chem.Phys.: (2006) **124** 214102.
122. Paricaud, P., Predota M., Chialvo A.A. and Cummings P.T., *From dimer to condensed phases at extreme conditions: Accurate predictions of the properties of water by a Gaussian charge polarizable model.* J. Chem. Phys.: (2005) **122** 244511.
123. Jackson, J.D., *Classical Electrodynamics*. 1975, New York: John Wiley & Sons.
124. Juffer, A.H., Botta E.F.F., Keulen B.A.M. van, Ploeg A. van der and Berendsen H.J.C., *The electric potential of a macromolecule in a solvent: a fundamental approach.* J.Comput.Phys.: (1991) **97** 144–171.
125. Eichinger, M., Tavan P., Hutter J. and Parrinello M., *A hybrid method for solutes in complex solvents: Density functional theory combined with empirical force fields.* J. Chem. Phys.: (1999) **110** 10452–10467.
126. Takahashi, H., Hori T., Hashimoto H. and Nitta T., *A hybrid QM/MM method employing real space grids for QM water in the TIP4P water solvents.* J.Comput.Chem.: (2001) **22** 1252–1261.

127. Müller, W., Flesch J. and Meyer W., *Treatment of intershell correlation effects in ab intio calculations by use of core potentals. Method and application to alkali and earth atoms.* J. Chem. Phys.: (1984) **80** 3297–3310.
128. Frecer, V. and Miertus S., *Polarizable continuum model of solvation for biopolymers.* Int. J.Quant. Chem.: (1992) **42** 1449–1468.
129. Willetts, A., Rice J.E., Burland D.M. and Shelton D.P., *Problems in the comparison of theoretical and experimental hyperpolarizabilities.* J. Chem Phys.: (1992) **97** 7590–7599.
130. Shelton, D.P. and Rice J.E., *Measurements and Calculations of the Hyperpolarkabilities of Atoms and Small Molecules in the Gas Phase.* Chem. Rev.: (1994) **94** 3–29.
131. Wortmann, R. and Bishop D.M., *Effective polarizabilities and local field corrections for nonlinear optical experiments in condensed media.* J.Chem.Phys.: (1998) **108** 1001–1007.
132. Lorentz, H.A., *The Theory of Electrons*. 1st. ed. 1909, Leizig: B.G. Teubner.
133. Boyd, R.W., *Nonlinear Optics*. 1992, San Diego: Academic Press.
134. Prasad, P.N. and Williams D.J., *Introduction to Nonlinear Optical Effeects in Molecules and Polymers*. 1991, New York: Wiley.
135. Butcher, P..N and Cotter D, *The Elements of Nonlinear Optics*. 1st ed. 1990, Cambridge: Cambridge University Press.
136. Jensen, L. and Duijnen P. Th. van, *The Discrete Solvent Reaction Field model: A Quantum mechanics/Molecular mechanics model for calculating nonlinear optical properties of molecules in the condensed phase.*, in Atoms, molecules and clusters in electric fields. Theoretical approaches to the calculation of electric polarizability, G. Maroulis, Editor. 2006, Imperial College Press: London. p. 1–43.
137. Duijnen, P.Th. van and Rullmann J.A.C., *Intermolecular interactions with the direct reaction field method.* Int. J. Quantum Chem.: (1990) **38** 181–189.
138. Dunning, T.H. and Hay P.J., *Gaussian basis sets for molecular calculations*, in Methods in Electronic Structure Theory, H.F. Schaefer III, Editor. 1977, Plenum: New York. p. 1–27.
139. Soper, A.K., *The radial distribution functions of water and ice from 220 to 673 K and at pressures up to 400 MPa.* Chem. Phys.: (2000) **258** 121–137.
140. Neusser, H.J. and Krause H., *Binding Energy and Structure of van der Waals Complexes of Benzene.* Chem. Rev.: (1994) **94** 1829–1843.
141. Sinnokrot, M.O. and Sherrill C.D., *Highly Accurate Coupled Cluster Potential Energy Curves for the Benzene Dimer: Sandwich, T-Shaped, and Parallel-Displaced Configurations.* J. Phys. Chem. A: (2004) **108** 10200–10207.
142. Swart, M., Wijs T. van der, Guerra C.Fonseca and Bickelhaupt F. M., *π-π stacking tackled with density functional theory.* J. Molec. Model.: (2007) in press.
143. Battaglia, M.R., Buckingham A.D. and Williams J.H., *The electric quadrupole moments of benzene and hexafluorobenzene.* Chem. Phys. Lett.: (1981) **78** 421–423.
144. Arunan, E. and Gutowsky H.S., *The rotational spectrum, structure and dynamics of a benzene dimer.* J.Chem.Phys.: (1993) **98** 4294–4296.
145. Kolos, W. and Roothaan C.C J., *Accurate Electronic Wave Functions for the H2 Molecule.* Rev. Mod. Phys.: (1960) **32,** 219–232.
146. Chalasinski, G., Szczesniak M.M., Cieplak P. and Scheiner S., *Ab initio study of intermolecular potential of Hz0 trimer.* J. Chem. Phys.: (1991) **94** 2873–2882.
147. Dunning, T.H., *Gaussian basis sets for use in correlated molecular calculations. I. The atoms boron through neoen and hydrogen.* (1989) **90** 1007–1023.
148. Schuddeboom, W., Jonker S.A., Warman J.M., Haas M.P. de, Vermeulen M.J.W., Jager W.F., Lange B. de, Feringa B.L. and Fessendens R.W., *Sudden Polarization in the Twisted, Phantom*

State of Tetraphenylethylene Detected by Time-Resolved Microwave Conductivity. J. Am. Chem. SOC: (1993) **115** 3286–3290.

149. Schilling, C.L. and Hilinski∗ E.F., *Dependence of the Lifetime of the Twisted Excited Singlet State of Tetraphenylethylene on Solvent Polarity.* J. Am .Chem.SOc.: (1988) **110** 2296–2298.
150. Ma, J. and Zimmt M.B., *Equilibration between the fluorescent and zwitterionic phantom states in alkyl-substituted tetraphenylethylenes.* J. Am .Chem.SOc.: (1992) **114** 9723–9724.
151. Zijlstra, R. W.J., Grozema F. C., Swart M., Feringa B. L. and Duijnen P. Th. van, *Solvent Induced Charge Separation in the Excited States of Symmetrical Ethylene: A Direct Reaction Field Study.* J.Phys.Chem.A: (2001) **105** 3583–3590.
152. Zijlstra, R.W.J., Duijnen P.Th. van, Feringa B.L., Steffen T., Duppen K. and Wiersma D.A., *Excited state dynamics of tetraphenylethene: ultrafast Stoke shift, isomerization and charge separation.* J.Phys.Chem.A: (1997) **101** 9828–9836.
153. Grozema, F.C., M.Swart, Zijlstra R.J.W., Piet J.J., Siebbeles L.D.A. and Duijnen P. Th. van, *QM/MM study of the role of the solvent in the formation of the charge separated excited state in 9,9'-bianthryl.* J. Am .Chem.SOc.: (2005) **127** 11019–11028.
154. Vries, A.H. de and Duijnen P.Th. van, *Solvatochroism of the $\pi*¨n$ transition of acetone by combined quantum mechanical–classical mechanical calculations.* Int. J. Quantum Chem.: (1996) **57** 1067–1076.
155. Duijnen, P.Th. van and Netzel T.L., *Explicit Solvent DRF INDOs/CIS Computations of Charge Transfer State Energetics in a Pyrenyldeoxyuridine Nucleoside Model.* J.Phys. Chem. A: (2006) **110** 2204–2213.
156. Mitchell, C.D. and Netzel T.L., *CIS INDO/S SCRF study of electron transfer excige states in a 1-pyrenyl substituted 1-methyluracil-5-carboxamide nucleoside: dielctric continuum solvation effects on electron transger states.* J.Phys.Chem. B: (2000) **104** 125–136.
157. Duijnen, P.Th. van, *ZINDO/DRF*, in *ZINDO, A General Semi-empirical Program Package*, M.C. Zerner, Editor. 1998, Quantum Theory Project, University of Florida: Gainesville (Fl.) USA. p. unpublished.
158. Duijnen, P.Th. van, *ZINDO/DRF_RUMER_CI*, in *ZINDO, A General Semi-empirical Program Package*, M.C. Zerner, Editor. 2003, Quantum Theory Project, University of Florida: Gaines-Gainesville (Fl.) USAville. p. unpublished.
159. Manne, R. and Zerner M.C., *Matrix elements of spin-dependent one-electron operators between bonded functions.* Int. J. Quantum Chem.Quantum Chemistry Symposium: (1986) **19** 165–172.
160. Duijnen, P.Th. van, Greene S.N. and Richards N.G.J., *Time dependent density functional theory/discrete reaction field spectra of open-shell systems: the visual spectrum of $[Fe^{III}(PyPepS)_2]^-$ in aqueous solution.* J.Chem.Phys.: (2007) **127** 045105.
161. Hirata, S. and Head-Gordon M., *Time-dependent density functional theory within the Tamm– Dancoff approximation.* Chem.Phys.Lett.: (1999) **314** 291–299.
162. Rinkevicius, Z., Tunell I., Salek P., Vahtras O. and Ågren H., *Restricted DFT theory of linear time-depnendent properties in open- shell molecules.* J. Chem. Phys.: (2003) **119** 34–46.
163. Wang, F. and Ziegler T., *Excitation energies of some d1 systems calculated using time-dependent density functional theory: an implementation of open-shell TDDFT theory for doublet–doublet excitations.* Mol.Phys: (2004) **102** 2585 – 2595.
164. Jensen, L., M.Swart, Duijnen P.Th. van and Autschbach J., *The circular dichroism spectrum of [Co(en)3] 3+ in water.* Int. J. Quantum Chem.: (2006) **106** 2479–2488.
165. Cammi, R., Cossi M. and Tomasi J., *Analytical derivatives for molecular solutes. III. Hartree – Fock static polarizability and hyperpolarizabilities in the polarizable continuum model.* J. Chem Phys.: (1996) **104** 4611–4620.

166. Luo, Y., Norman P. and Ågren H., *A semiclassical approximation model for properties of molecules in solution.* J. Chem. Phys.: (1998) **109** 3589–3595.
167. Dehu, C., Geskin V., Persoons A. and Brédas J.-L., *Effect of medium polarity on the secnd order polarizabiity of an ocupolar chromophore: an ab initio reation field study.*. Eur. J. Org. Chem.: (1998) 1267–1269.
168. Morita, A. and Kato S., *An ab initio analysis of medium perturbation on molecular polarizabilities.* J.Chem.Phys.: (1999) **110** 11987–11998.
169. Jensen, L. and Duijnen P.Th. van, *The first hyperpolarizability of p-nitroaniline in 1,4-dioxane: A quantum mechanical/molecular mechanics study.* J. Chem. Phys.: (2005) **213** 074307.
170. Mikkelsen, K.V., Luo Y., H.Ågren and Jørgensen P., *Sign change of hyerpolarizablities of solvated water.* J. Chem Phys.: (1995) **102** 9362–9367.
171. Kaatz, P. and Shelton D.P., *Polarized hyper-Rayleigh light scattering measurements of nonlinear optical chromophores.* J. Am .Chem.SOc.: (1996) **105** 3918–3929.
172. Shoji, I., Kondo T. A. and Ito R., *Second-order nonlinear susceptibilities of various dielectric and semiconductor materials.* Opt.Quantum Electr.: (2002) **34** 797–833.
173. Stähelin, M., Burland D.M. and Rice J.E., *Solvent dependence of the second order hyperpolarizability in p-nitroaniline.* Chem. Phys. Lett.: (1992) **191** 245–250.
174. Connolly, M.L., *Solvent-accessible surface of proteins and nucleic acids.* Science: (1983) **221** 709–713.
175. Pierotti, R.A., *A scaled particle theory of aqueous and nonaqueous solutions.* Chem. Rev.: (1976) **76** 717–726.
176. Winstein, S. and Fainberg A.H., *Correlation of Solvolysis Rates. 1 V.l Solvent Effects on Enthalpy and Entropy of Activation for Solvolysis of &Butyl Chloride2.* J. Am .Chem.Soc.: (1957) **79** 5937–5950.
177. Winstein, S., Clippinger E., Fainberg A.H. and Robinson G.C., *Salt effexts of ion-pairs in solvolysis.* J.Am.Chem.Soc.: (1954) **76** 2597.
178. Remko, M., Duijnen P.Th. van and Lieth C-W. von der, *Structure and stability of Li (I) and Na(I) - carboxylate, sulfate and phosphate complexes.* J.Mol.Struct. (THEOCHEM): (2007) **814** 119–125.
179. Remko, M., Duijnen P.Th. van and Swart M., *Theoretical study of molecular structure, tautomerism, and geometrical isomerism of N-methyl and N-phenyl substituted cyclic imidazolines, oxazolines and thiazolines.* Struct.Chem.: (2003) **14** 271–278.
180. Calvert, J. G. and Pitts J. N., *Photochemistry*. 1966, New York: Wiley. 377.
181. Hayes, W.P. and Timmons C.J., *Solvent and substituent effects on the nÆπ∗ absorption bands of some ketones.* Spectrochim. Acta: (1965) **21** 529–541.
182. Bayliss, N.S. and Wills-Johnson G., *Solvent effects on the intensities and weak ultraviolet spectra of ketones and nitroparaffins - I.* Spectrochim. Acta: (1968) **24A** 551–661.
183. Kajzar, F. and J.Messier, *Third-harmonic generation in liquids.* Phys. Rev. A: (1985) **32** 2352–2363.
184. Levine, B. F. and Bethea C. G., *Effects on hyperpolarizabilities of molecular interactions in associating liquid mixtures.* J. Chem. Phys.: (1976.) **65** 2429–2438.
185. Thormahlen, I., Straub J. and Grigul. U., *Refractive Index of Water and Its Dependence on Wavelength, Temperature, and Density.* J. Phys. Chem. Ref. Data: (1985) **14** 933–945.
186. Teng, C.C. and Garito A.F., *Dispersion of the nonlinear second-order optical susceptibility of organic systems.* Phys. Rev. B: (1983) **28** 6766–6773.
187. Grozema, F.C. and Duijnen P.Th. van, *Solvent effects on the π∗◇n transition in various solvents.* J.Phys.Chem.A: (1998) **102** 7984–7989.